J. Plasma Phys. (2024), *vol*. 90, 905900621
Published by Cambridge University Press

doi:10.1017/S0022377824000953

Statistical theory of the broadband two-plasmon decay instability

R.T. Ruskov [1],†, R. Bingham [2,3], L.O. Silva [1,4], M. Harper[5], R. Aboushelbaya [1], J.F. Myatt [6] and P.A. Norreys [1,7]

[1]Department of Physics, Atomic and Laser Physics sub-Department, University of Oxford, Clarendon Laboratory, Parks Road, Oxford OX1 3PU, UK

[2]UKRI-STFC Central Laser Facility, Rutherford Appleton Laboratory, Didcot OX11 0QX, UK

[3]Department of Physics, University of Strathclyde, John Anderson Building, 107 Rottenrow East, Glasgow G4 0NG, UK

[4]GoLP/Instituto de Plasmas e Fusão Nuclear, Instituto Superior Técnico, Universidade de Lisboa, 1049-001 Lisboa, Portugal

[5]St Hilda's College, University of Oxford, Cowley Place, Oxford OX4 1DY, UK

[6]Department of Electrical and Computer Engineering, University of Alberta, Edmonton, Alberta, BT6G 1H9, Canada

[7]John Adams Institute for Accelerator Science, University of Oxford, Denys Wilkinson Building, Keble Road, Oxford OX1 3RH, UK

(Received 26 April 2024; revised 5 August 2024; accepted 6 August 2024)

There is renewed interest in direct-drive inertial confinement fusion, following the milestone December 2022 3.15 MJ ignition result on the National Ignition Facility. A key obstacle is the control of the two-plasmon decay instability. Here, recent advances in inhomogeneous turbulence theory are applied to the broadband parametric instability problem for the first time. A novel dispersion relation is derived for the two-plasmon decay in a uniform plasma valid under broad-bandwidth laser fields with arbitrary power spectra. The effects of temporal incoherence on the instability are then studied. In the limit of large bandwidth, the well-known scaling relations for the growth rate are recovered, but it is shown that the result is more sensitive to the spectral shape of the laser pulse rather than to its coherence time. The range of wavenumbers of the excited plasma waves is shown to be substantially broadened, suggesting that the absolute instability is favoured in regions further away from the quarter critical density. The intermediate-bandwidth regime is explored numerically – the growth rate is reduced to half its monochromatic value for laser intensities of 10^{15} W cm^{-2} and relatively modest bandwidths of 5 THz. The instability-quenching properties of a spectrum of discrete lines spread over some bandwidth have also been studied. The reduction in the growth rate is found to be somewhat lower compared with the continuous case but is still significant, despite the fact that, formally, the coherence time of such a laser pulse is infinite.

Key words: plasma instabilities, plasma nonlinear phenomena, fusion plasma

† Email address for correspondence: rusko.ruskov@physics.ox.ac.uk

1. Introduction

Very significant progress has recently been made at the Lawrence Livermore National Laboratory in the generation of high-energy-density conditions required for fusion energy gain. The August 2021 experiment, where a fusion yield of 1.3 MJ was obtained on the National Ignition Facility, confirmed that the Lawson criterion had been satisfied for the first time (Abu-Shawareb *et al.* 2022; Zylstra *et al.* 2022). Subsequently, in December 2022, more energy was released in fusion products than was delivered to target, with exquisite measurements of a 3.12 MJ yield (Abu-Shawareb *et al.* 2024). These results mark a major milestone in the progress of inertial confinement fusion (ICF) research, which have reinvigorated worldwide efforts to explore routes to higher fusion gain for applications such as nuclear stockpile stewardship and inertial fusion energy.

One of the leading contenders for higher gains at current laser facility energy levels is the direct-drive ICF approach, principally due to the significantly larger energy coupling to the target that results in higher hydrodynamic efficiency of the implosions (Craxton *et al.* 2015; Campbell *et al.* 2021). A major problem for direct-drive ICF is the generation of highly energetic (hot) electrons which can prematurely raise the temperature of the fusion fuel and subsequently degrade the implosion performance. The source of these hot electrons are parametric instabilities that are driven as the laser beams propagate through the coronal plasma surrounding the target. When one of the decay products of a parametric instability is an electron plasma wave – as is the case for the two-plasmon decay (TPD) instability – hot electrons are generated (Vu *et al.* 2012*a*,*b*). The fraction of laser energy converted into hot electrons has to be limited to about 0.1 % for a successful implosion (Craxton *et al.* 2015).

Progress in the understanding of the impact of TPD on ICF experiments has been considerable in the recent years. The TPD instability is a three-wave instability in which an electromagnetic wave decays into a pair of electron plasma waves. Frequency matching between the waves is possible only in a spatially localised region near the quarter critical density (figure 1*a*). Hot electron generation typically occurs when the instability is in the so-called absolute regime in which wave amplitudes grow exponentially at a fixed point in space; saturation therefore only occurs through nonlinear processes, resulting in a plasma in a highly turbulent state, which accelerates the electrons stochastically (DuBois, Russell & Rose 1995; DuBois, Rose & Russell 1996; Vu *et al.* 2012*a*,*b*). When multiple laser beams are arranged in a cone (as is the case in real experimental facilities) they can cooperatively drive the instability by sharing a common plasma wave along the axis of symmetry (DuBois, Bezzerides & Rose 1992) (see figure 1*b*). This results in substantial TPD growth even when the single beam thresholds are far from exceeded (Michel *et al.* 2013; Myatt *et al.* 2014). While the shared plasma wave along the cone axis is high-k and grows convectively, it has been shown recently that multiple laser beams can drive a low-k absolute mode cooperatively, with a lower threshold compared with the high-k one (Zhang *et al.* 2014). Simulations and experiments of hot electrons driven by the multi-beam TPD instability show that the fraction of laser energy converted into hot electrons is near 0.1 % at overlapped intensities of about $10^{15}\,\mathrm{W\,cm^{-2}}$, rising to about 1 % at $1.5 \times 10^{15}\,\mathrm{W\,cm^{-2}}$ (Follett *et al.* 2017). In addition to generating hot electrons, TPD has been recently shown to be responsible for a large amount of anomalous absorption of laser energy (up to $\simeq$30 %) near the quarter critical density region (Seka *et al.* 2014; Turnbull *et al.* 2020). This is likely to be problematic as it increases the distance over which thermal energy needs to be conducted through in order to reach the ablation surface. Taming laser plasma instabilities at high intensities is therefore highly beneficial for direct-drive target designs (Paddock *et al.* 2021, 2022; Schmitt & Obenschain 2023*a*,*b*; Trickey *et al.* 2024).

https://doi.org/10.1017/S0022377824000953 Published online by Cambridge University Press

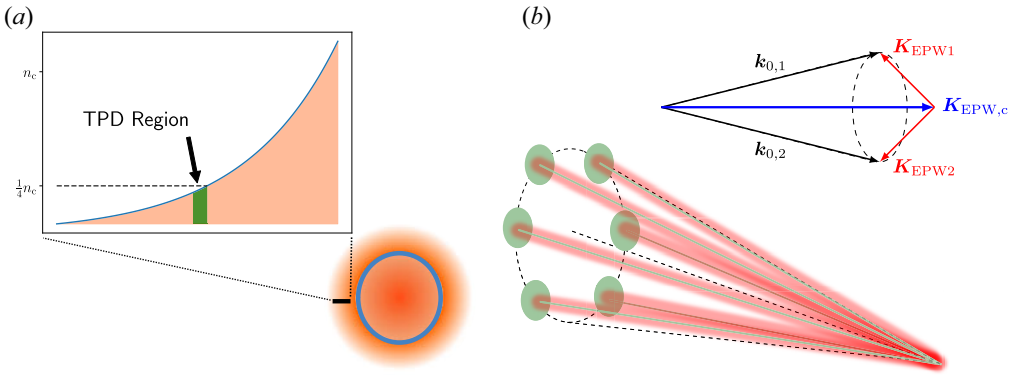

FIGURE 1. (*a*) An illustration of an imploding ICF pellet, together with its surrounding coronal plasma. The plot shows an illustration of the density gradient in the corona and the region near the quarter critical density where the TPD instability is excited. (*b*) An illustration of a set of six laser beams arranged in a cone, as well as a wavevector diagram showing how, due to the cone geometry, a pair of electromagnetic waves ($\boldsymbol{k}_{0,1}$ and $\boldsymbol{k}_{0,2}$) can share a plasma wave along the cone axis ($\boldsymbol{K}_{\mathrm{EPW},c}$, in blue). The wavenumber matching condition due to the jth beam in the cone is $\boldsymbol{k}_{0,j} = \boldsymbol{K}_{\mathrm{EPW},c} + \boldsymbol{K}_{\mathrm{EPW}j}$, where $\boldsymbol{K}_{\mathrm{EPW}j}$ (in red) is the second plasma wave involved in TPD which is distinct for each beam.

It has been known for some time that increasing the temporal bandwidth of the driving laser pulse significantly reduces the growth rates and increases the thresholds for the onset of parametric instabilities (Thomson & Karush 1974; Thomson 1975; Laval, Pellat & Pesme 1976; Obenschain, Luhmann & Greiling 1976; Laval *et al.* 1977; Lu 1988, 1989; DuBois *et al.* 1992; Pesme *et al.* 1992). The Omega Laser Facility at the Laboratory for Laser Energetics is currently undergoing the FLUX upgrade (Dorrer, Hill & Zuegel 2020; Dorrer *et al.* 2021) in which fractional bandwidths of up to $\Delta\omega/\omega_0 = 1$–$2\,\%$ will be generated in order to experimentally test these ideas (Turnbull *et al.* 2023). Bandwidths of such order are expected to mitigate all laser plasma instabilities in Omega experiments (Follett *et al.* 2021; Bates *et al.* 2023). Here $\Delta\omega$ is the full width at half maximum of the laser power spectrum, and ω_0 the frequency around which it is centred. The thresholds for the onset of parametric instabilities are typically set by inhomogeneity, and calculating them is of great importance. Follett *et al.* (2019) recently compared the analytic model of Lu (1989) based on their effective Hamiltonian method against simulations utilising the Laser Plasma Simulation Environment (LPSE) code (Myatt *et al.* 2017), and found disagreements as large as a factor of $\sim$20 times in the case of the TPD threshold. Given the great promise of controlling laser plasma instabilities with laser bandwidth, it is crucial that theoretical models describe the results of experiments and simulations well, and in some of the most important cases (absolute TPD and Raman scattering) the reliability of current models is somewhat uncertain.

The broadband parametric instability problem suffers from complications similar to those involved in the study of turbulence. Laser bandwidth introduces fluctuations in the laser pulse electric field whose minute details are unknown or too difficult to describe. Hence a statistical approach to the problem must be pursued, only seeking to model some small set of averaged properties of the fluctuations – for example their spectra. But difficulties arise as one attempts to carry out statistical predictions about a system's evolution, and one is frequently faced with the statistical closure problem (Krommes 2002, 2015; Krommes & Parker 2019). Most statistical closures such as the commonly

https://doi.org/10.1017/S0022377824000953 Published online by Cambridge University Press

used random phase approximation (Nazarenko 2011; Connaughton, Nazarenko & Quinn 2015) assume homogeneous statistics – meaning that the statistical properties of the fields of interest do not vary in space. This immediately causes trouble if one is interested in analysing convective growth or non-uniform plasmas – both of which are crucially important for understanding parametric instabilities (Michel 2023). As discussed below it is also problematic even in a uniform plasma, when a zero-order perturbation is present.

Lately there has been some significant progress in moving beyond homogeneous statistical closures. For example, the quasi-linear interaction of inhomogeneous turbulence with plasma has been a long-standing problem where only recently a definitive theory was put forward (Dodin 2022). Similarly substantial developments in the theory of drift-wave turbulence interacting with zonal flows in tokamaks have been enabled by new insights about how to properly model the inhomogeneous statistics of the turbulent fields (Parker 2014; Krommes 2015; Parker 2016; Ruiz *et al.* 2016; Krommes & Parker 2019; Ruiz, Glinsky & Dodin 2019; Zhu 2020; Zhu, Zhou & Dodin 2020; Zhu & Dodin 2021), improving upon initial work based on the traditional wave-kinetic approach (Smolyakov, Diamond & Shevchenko 2000; Trines *et al.* 2005, 2007, 2009). This drift-wave zonal-flow (DW-ZF) problem which is thought important in regulating turbulent transport in tokamaks, also bears resemblance to that of the broadband parametric instabilities in the sense that both seek to describe instabilities of some broad spectrum of waves – the drift-wave turbulence on the one hand, and the broad spectrum of electromagnetic waves on the other.

Here a statistical theory of the broadband TPD instability in a homogeneous plasma is presented for the first time, valid under laser fields with arbitrary power spectra. The same closure procedure as that used to study the DW-ZF problem is applied, namely the second-order cumulant expansion, also known as CE2, which allows for inhomogeneous statistics. Despite the fact that here one does not impose a density gradient, this is still crucial as inhomogeneity in statistics arises due the strong partially incoherent electromagnetic mode, i.e. the broadband laser pulse which is considered a zero-order perturbation (DuBois & Bezzerides 1976; DuBois 2000). The CE2 closure captures the exact coupling of the stochastic fluctuations to the mean field, and ignores all cumulants of order ≥ 3.[1] This implies that the stochastic fluctuations follow (jointly) normal distributions, and that they interact quasi-linearly with the mean field. The Weyl symbol calculus (McDonald 1988; Tracy *et al.* 2014; Dodin 2022) is employed in this article, which greatly facilitates the derivation of the equations governing the correlation functions. This new work is a generalisation of the approach of Santos, Silva & Bingham (2007), which considered the broadband Raman scattering instability.[2] Their key insight was that extending the Wigner–Moyal formalism of quantum mechanics provides a natural statistical framework for describing laser pulse propagation inside the plasma, resulting in their generalised photon kinetics model (Santos & Silva 2005; Silva & Bingham 2013). Generalised photon kinetics is, in essence, the Wigner–Moyal representation of the Klein–Gordon equation which describes laser pulse propagation in a plasma. They did not face a closure problem as they assumed the electrostatic fluctuations associated with electron plasma waves to be non-random. In the case of the TPD this is not possible, and one has to provide a statistical description of the plasma as well. It should be noted that

[1]The first- and second-order cumulants of a distribution are given by its first and second moments. The cumulants of order $n \geq 3$ are the difference between the nth moment and the value it would have had if the distribution were a Gaussian with the mean and variance implied by the first- and second-order cumulants. This implies that, for a Gaussian distribution, all cumulants of order $n \geq 3$ vanish.

[2]With slight modifications of the same model, the stimulated Brillouin scattering instability has also been studied by Brandão *et al.* (2021).

https://doi.org/10.1017/S0022377824000953 Published online by Cambridge University Press

were they to allow for stochasticity of the plasma, then they would effectively use the same closure as the one described here, and their model would have the same statistical content as the new one presented here.

The paper is organised as follows. In § 2 the dispersion relation for the TPD instability is derived, one that is valid for laser fields with arbitrary power spectra in a uniform plasma. Emphasis is made on the details of the statistical closure. In § 3 the broadband dispersion relation is applied to some cases of interest – namely, it is shown that it reduces to the well-known dispersion relation for a single monochromatic beam, as well as multiple monochromatic non-interfering ones; following that, the effects of temporal incoherence on the instability as driven by a single broadband laser beam are considered; and lastly the extent to which a laser power spectrum consisting of multiple discrete spectral lines spread over a bandwidth $\Delta\omega$ approximates the instability-quenching properties of a continuous spectrum is explored. To conclude the article, a summary and a discussion of the new results are presented in § 4.

2. Model

The TPD instability is a three-wave parametric instability in which an electromagnetic wave decays into a pair of plasma waves. Due to the Manley–Rowe relations, the frequencies and wavenumbers of the interacting waves must be matched (Michel 2023). This localises the instability spatially near the quarter critical density – the point where the laser frequency is equal to twice the local plasma frequency (see figure 1*a*). Furthermore, since all of the waves are high in frequency, the ion motion can be neglected in the linear stage of the instability. The response of the electrons in the presence of the laser field can be analysed using non-relativistic fluid equations. Kinetic effects can be ignored provided $k\lambda_{De} \ll 1$. Relativistic effects are negligible under conventional hot-spot ignition ICF where the laser intensity is of order $I_L \sim 10^{15}\,\mathrm{W\,cm^{-2}}$ and the laser wavelength is $\lambda_L \sim 350\ \mu\mathrm{m}$. This is because the quiver velocity of the electrons $\boldsymbol{v}_{\mathrm{os}}(t,\boldsymbol{x}) = e\boldsymbol{A}_0/m_e$ in the presence of an electromagentic wave described by the vector potential $\boldsymbol{A}_0(t,\boldsymbol{x})$ is $v_{\mathrm{os}}/c \sim 0.01$ under such conditions. Finally, for the motion of the ions to be neglected, we need the amplitude of electrostatic waves to be low enough such that $\sqrt{W_e} \ll k\lambda_{De}$, where $W_e = \frac{1}{2}\epsilon_0|\boldsymbol{\nabla}\varphi|^2/n_eT_e$. This ensures that the nonlinear terms which couple the electron and ion motion are of higher order and negligible. So, the following ordering will be assumed from now on:

$$\sqrt{\frac{\epsilon_0|\boldsymbol{\nabla}\varphi|^2}{2n_eT_e}} \ll \frac{v_{\mathrm{os}}}{c} \sim k\lambda_{De} \ll 1. \tag{2.1}$$

Assuming a purely electrostatic perturbation, linearising the continuity and momentum equations for the electron fluid gives (Liu & Rosenbluth 1976; Simon *et al.* 1983)

$$\left.\begin{aligned} \frac{\partial n}{\partial t} &= -\nabla^2\psi - \boldsymbol{v}_{\mathrm{os}}\cdot\boldsymbol{\nabla}n, \\ \frac{\partial\psi}{\partial t} &= \omega_{\mathrm{pe}}^2\nabla^{-2}n - 3v_{\mathrm{the}}^2 n - \boldsymbol{v}_{\mathrm{os}}\cdot\boldsymbol{\nabla}\psi. \end{aligned}\right\} \tag{2.2}$$

Here $n(t,\boldsymbol{x})$ is the electron density perturbation normalised to the equilibrium density n_0 which will be assumed uniform for simplicity, $\psi(t,\boldsymbol{x})$ is the velocity potential of the electrons meaning $\boldsymbol{u} = \boldsymbol{\nabla}\psi$, where $\boldsymbol{u}$ is the electron fluid velocity, $\omega_{\mathrm{pe}}^2 = e^2n_0/\epsilon_0m_e$ is the equilibrium plasma frequency and $v_{\mathrm{the}}^2 = T_e/m_e$ is the electron thermal velocity. Since the goal is to develop a description of the instability under broad-bandwidth (stochastic) laser fields, n, ψ and $\boldsymbol{v}_{\mathrm{os}}$ are assumed to be random variables.

https://doi.org/10.1017/S0022377824000953 Published online by Cambridge University Press

The wave equation governing the electron plasma waves is

$$\left(\frac{\partial^2}{\partial t^2}+\omega_{\rm pe}^2-3v_{{\rm the}}^2\nabla^2\right)n=\nabla^2(\boldsymbol{v}_{\rm os}\cdot\nabla\psi)-\frac{\partial}{\partial t}(\boldsymbol{v}_{\rm os}\cdot\nabla n), \tag{2.3}$$

where the right-hand side contains the TPD driving terms. One can express the driving terms through the Wigner functions describing the correlations between the pump field $\boldsymbol{v}_{\rm os}$ and the plasma waves, as has been done in the case of inhomogeneous Navier–Stokes turbulence (Tsiolis, Zhou & Dodin 2020) (see Appendix B):

$$\boldsymbol{v}_{\rm os}\cdot\nabla\psi=\mathrm{i}\int\frac{\mathrm{d}\boldsymbol{k}}{(2\pi)^3}\boldsymbol{k}^{\top}\star\mathbf{W}_{\psi\boldsymbol{v}}^{\top}. \tag{2.4}$$

Here $\mathbf{W}_{\psi\boldsymbol{v}}(\boldsymbol{x},\boldsymbol{k})=\mathscr{W}[|\psi\rangle\langle\boldsymbol{v}_{\rm os}|]$, with $\mathscr{W}$ being the Wigner transform, and the bra-ket notation is used as in Dodin (2022); $\mathbf{W}_{\psi\boldsymbol{v}}^{\mathsf{T}}$ denotes the transpose of $\mathbf{W}_{\psi\boldsymbol{v}}$. The Wigner transform $\mathscr{W}[\hat{A}]$ of some generic operator $\hat{A}$ is called the Weyl symbol of $\hat{A}$, and is defined as

$$\mathsf{A}(\boldsymbol{x},\boldsymbol{k})\equiv\mathscr{W}[\hat{A}]\doteq\int\mathrm{d}\boldsymbol{s}\,\mathrm{e}^{-\mathrm{i}\boldsymbol{k}\cdot\boldsymbol{s}}\left\langle\boldsymbol{x}+\frac{\boldsymbol{s}}{2}\middle|\,\hat{A}\,\middle|\boldsymbol{x}-\frac{\boldsymbol{s}}{2}\right\rangle. \tag{2.5}$$

The Moyal star product $\star$ between two symbols is defined as $\mathsf{A}\star\mathsf{B}\doteq\mathscr{W}[\hat{A}\hat{B}]$; it is given by $\mathsf{A}(\boldsymbol{x},\boldsymbol{k})\star\mathsf{B}(\boldsymbol{x},\boldsymbol{k})=\mathsf{A}(\boldsymbol{x},\boldsymbol{k})\,\mathrm{e}^{\mathrm{i}\hat{\mathcal{P}}/2}\mathsf{B}(\boldsymbol{x},\boldsymbol{k})$, with $\hat{\mathcal{P}}$ being the Poisson bracket $\hat{\mathcal{P}}=\overleftarrow{\partial}_{\boldsymbol{x}}\cdot\overrightarrow{\partial}_{\boldsymbol{k}}-\overleftarrow{\partial}_{\boldsymbol{k}}\cdot\overrightarrow{\partial}_{\boldsymbol{x}}$, and the arrows indicating the directions in which the derivatives are acting. Element-wise application of the Moyal star product $\star$ and the usual matrix multiplication rules are assumed, meaning that for any two matrix symbols $\mathbf{A}$ and $\mathbf{B}$ one applies the Moyal product as follows: $(\mathbf{A}\star\mathbf{B})_{ij}=\sum_k(\mathbf{A})_{ik}\star(\mathbf{B})_{kj}$. A brief introduction to the Weyl symbol calculus can be found in Appendix A. With these definitions, one can see that the quantity $\mathbf{W}_{\psi\boldsymbol{v}}(\boldsymbol{x},\boldsymbol{k})$ is given by

$$\mathbf{W}_{\psi\boldsymbol{v}}(\boldsymbol{x},\boldsymbol{k})=\int\mathrm{d}\boldsymbol{s}\,\mathrm{e}^{-\mathrm{i}\boldsymbol{k}\cdot\boldsymbol{s}}\psi(\boldsymbol{x}+\boldsymbol{s}/2)\boldsymbol{v}_{\rm os}^{\dagger}(\boldsymbol{x}-\boldsymbol{s}/2). \tag{2.6}$$

After ensemble averaging, $\mathbf{W}_{\psi\boldsymbol{v}}(\boldsymbol{x},\boldsymbol{k})$ will represent the correlations of the laser pulse field $\boldsymbol{v}_{\rm os}$ with the the velocity potential ψ. The second driving term is rewritten in a completely analogous manner leading to the quantity $\mathbf{W}_{n\boldsymbol{v}}(\boldsymbol{x},\boldsymbol{k})$ which will represent the correlations between $\boldsymbol{v}_{\rm os}$ and the density perturbation n.

Taking the Fourier transform of the wave equation, and ensemble averaging, leads to

$$D_e(\Omega,\boldsymbol{K})\mathring{\bar{n}}(\Omega,\boldsymbol{K})=\int\frac{\mathrm{d}\boldsymbol{k}}{(2\pi)^3}\left(\boldsymbol{k}-\tfrac{1}{2}\boldsymbol{K}\right)\cdot\left(\mathrm{i}K^2\mathring{\bar{\mathbf{W}}}_{\psi\boldsymbol{v}}-\Omega\mathring{\bar{\mathbf{W}}}_{n\boldsymbol{v}}\right), \tag{2.7}$$

where $D_e(\Omega,\boldsymbol{K})=\Omega^2-\omega_{\rm pe}^2-3v_{{\rm the}}^2K^2=\Omega^2-\omega_{e\boldsymbol{K}}^2$ is the dispersion function for the electron plasma waves, and the Fourier transformed quantities are denoted as follows: $\mathring{n}(\Omega,\boldsymbol{K})=\int\mathrm{d}t\mathrm{d}\boldsymbol{x}\,n(t,\boldsymbol{x})\,\mathrm{e}^{\mathrm{i}\Omega t-\mathrm{i}\boldsymbol{K}\cdot\boldsymbol{x}}$. The overline represents ensemble averaging. Here one now faces the closure problem – to calculate the mean field $\bar{n}$, knowledge is needed of second-order quantities: $\bar{\mathbf{W}}_{\psi\boldsymbol{v}}$ and $\bar{\mathbf{W}}_{n\boldsymbol{v}}$. The powerful toolbox of the Weyl symbol calculus is now applied to derive and solve the equations governing these quantities.

The basic idea is as follows: if one writes down the governing equations of the system in Schrödinger form, then all of the second-order correlation functions describing the system will be governed by the Wigner–Moyal equation (see Appendix A). A similar procedure was carried out for the case of inhomogeneous fluid turbulence by Tsiolis *et al.* (2020).

https://doi.org/10.1017/S0022377824000953 Published online by Cambridge University Press

The TPD equations (2.2) are first order in time and are readily put in Schrödinger form. The vector potential $\boldsymbol{A}_0$ describing the propagation of an electromagnetic mode in a plasma obeys a Klein–Gordon equation and therefore $(\partial_t^2 - c^2\nabla^2 + \omega_{\mathrm{pe}}^2)\boldsymbol{v}_{\mathrm{os}} = 0$, since $\boldsymbol{v}_{\mathrm{os}}$ differs from $\boldsymbol{A}_0$ only by a constant factor (Kruer 2019; Michel 2023). There are no source or sink terms in this equation since the linear stage of the instability is considered and hence pump depletion is ignored. This second-order-in-time equation can be decomposed into two first-order ones by defining the auxiliary fields $\boldsymbol{\phi}$, $\boldsymbol{\chi} = \frac{1}{2}(\boldsymbol{v}_{\mathrm{os}} \pm \mathrm{i}\omega_{\mathrm{pe}}^{-1}\partial_t \boldsymbol{v}_{\mathrm{os}})$ (Santos & Silva 2005).

The system of the decomposed Klein–Gordon equation, together with the two TPD equations are then written as a Schrödinger equation, $\mathrm{i}\partial_t \boldsymbol{\Psi} = \widehat{\boldsymbol{H}}\boldsymbol{\Psi}$, with the following matrix Hamiltonian and state vector:

$$\widehat{\boldsymbol{H}} = \begin{pmatrix} 0 & -\mathrm{i}\nabla^2 & -\mathrm{i}\boldsymbol{\eta}^\top & -\mathrm{i}\boldsymbol{\eta}^\top \\ \mathrm{i}(\omega_{\mathrm{pe}}^2\nabla^{-2} - 3v_{\mathrm{the}}^2) & 0 & -\mathrm{i}\boldsymbol{u}^\top & -\mathrm{i}\boldsymbol{u}^\top \\ 0 & 0 & -\dfrac{c^2}{2\omega_{\mathrm{pe}}}\nabla^2 + \omega_{\mathrm{pe}} & -\dfrac{c^2}{2\omega_{\mathrm{pe}}}\nabla^2 \\ 0 & 0 & \dfrac{c^2}{2\omega_{\mathrm{pe}}}\nabla^2 & \dfrac{c^2}{2\omega_{\mathrm{pe}}}\nabla^2 - \omega_{\mathrm{pe}} \end{pmatrix}, \quad \boldsymbol{\Psi} = \begin{pmatrix} n \\ \psi \\ \boldsymbol{\phi} \\ \boldsymbol{\chi} \end{pmatrix}, \tag{2.8a,b}$$

where $\boldsymbol{\eta} \doteq \nabla n$ and $\boldsymbol{u} \doteq \nabla\psi$. The Wigner matrix $\mathbf{W} = \mathscr{W}[|\boldsymbol{\Psi}\rangle\langle\boldsymbol{\Psi}|]$ satisfies the Wigner–Moyal equation:

$$\mathrm{i}\partial_t \mathbf{W} = \mathbf{H} \star \mathbf{W} - \mathbf{W} \star \mathbf{H}^\dagger, \tag{2.9}$$

with $\mathbf{H} \doteq \mathscr{W}[\widehat{\boldsymbol{H}}]$ being the symbol of the matrix Hamiltonian. It is useful to write out the contents of the Wigner matrix and the symbol of the matrix Hamiltonian explicitly:

$$\mathbf{H} = \begin{pmatrix} 0 & \mathrm{i}k^2 & -\mathrm{i}\boldsymbol{\eta}^\top & -\mathrm{i}\boldsymbol{\eta}^\top \\ -\mathrm{i}k^{-2}\omega_{e\boldsymbol{k}}^2 & 0 & -\mathrm{i}\boldsymbol{u}^\top & -\mathrm{i}\boldsymbol{u}^\top \\ 0 & 0 & \dfrac{c^2}{2\omega_{\mathrm{pe}}}k^2 + \omega_{\mathrm{pe}} & \dfrac{c^2}{2\omega_{\mathrm{pe}}}k^2 \\ 0 & 0 & -\dfrac{c^2}{2\omega_{\mathrm{pe}}}k^2 & -\dfrac{c^2}{2\omega_{\mathrm{pe}}}k^2 - \omega_{\mathrm{pe}} \end{pmatrix}, \tag{2.10}$$

$$\mathbf{W} = \begin{pmatrix} \mathsf{W}_{nn} & \mathsf{W}_{n\psi} & \mathbf{W}_{n\boldsymbol{\phi}} & \mathbf{W}_{n\boldsymbol{\chi}} \\ \mathsf{W}_{\psi n} & \mathsf{W}_{\psi\psi} & \mathbf{W}_{\psi\boldsymbol{\phi}} & \mathbf{W}_{\psi\boldsymbol{\chi}} \\ \mathbf{W}_{\boldsymbol{\phi}n} & \mathbf{W}_{\boldsymbol{\phi}\psi} & \mathbf{W}_{\boldsymbol{\phi}\boldsymbol{\phi}} & \mathbf{W}_{\boldsymbol{\phi}\boldsymbol{\chi}} \\ \mathbf{W}_{\boldsymbol{\chi}n} & \mathbf{W}_{\boldsymbol{\chi}\psi} & \mathbf{W}_{\boldsymbol{\chi}\boldsymbol{\phi}} & \mathbf{W}_{\boldsymbol{\chi}\boldsymbol{\chi}} \end{pmatrix}, \tag{2.11}$$

where the quantities which have a vector index in the second slot such as $\mathbf{W}_{n\boldsymbol{\phi}}$ are row vectors; similarly $\mathbf{W}_{\boldsymbol{\phi}n}$ is a column vector; and quantities such as $\mathbf{W}_{\boldsymbol{\phi}\boldsymbol{\phi}}$ with two vector indices are matrices.

Note that the relevant Wigner functions in (2.7) are related to the components of this Wigner matrix above through $\mathbf{W}_{nv} = \mathbf{W}_{n\boldsymbol{\phi}} + \mathbf{W}_{n\boldsymbol{\chi}}$ and $\mathbf{W}_{\psi v} = \mathbf{W}_{\psi\boldsymbol{\phi}} + \mathbf{W}_{\psi\boldsymbol{\chi}}$, and so one needs only to compute the evolution equations of the upper right 2×2 corner of $\mathbf{W}$. Doing so and taking sums and differences of the equations in the resulting system, one

https://doi.org/10.1017/S0022377824000953 Published online by Cambridge University Press

gets equations for $\mathbf{W}_{nv}$ and $\mathbf{W}_{\psi v}$, which upon ensemble averaging results in the following system:

$$\left.\begin{aligned}
\mathrm{i}\partial_t \bar{\mathbf{W}}_{nv} &= \mathrm{i}k^2 \star \bar{\mathbf{W}}_{\psi v} - \mathrm{i}\bar{\boldsymbol{\eta}}^{\top} \star \bar{\mathbf{W}}_{vv} - \omega_{\mathrm{pe}} \bar{\mathbf{B}}_{nv}, \\
\mathrm{i}\partial_t \bar{\mathbf{B}}_{nv} &= \mathrm{i}k^2 \star \bar{\mathbf{B}}_{\psi v} - \mathrm{i}\bar{\boldsymbol{\eta}}^{\top} \star \bar{\mathbf{B}}_{vv} - \omega_{\mathrm{pe}}^{-1} \bar{\mathbf{W}}_{nv} \star \omega_{\boldsymbol{k}}^2, \\
\mathrm{i}\partial_t \bar{\mathbf{W}}_{\psi v} &= -\mathrm{i}k^{-2}\omega_{e\boldsymbol{k}}^2 \star \bar{\mathbf{W}}_{nv} - \mathrm{i}\bar{\boldsymbol{u}}^{\top} \star \bar{\mathbf{W}}_{vv} - \omega_{\mathrm{pe}} \bar{\mathbf{B}}_{\psi v}, \\
\mathrm{i}\partial_t \bar{\mathbf{B}}_{\psi v} &= -\mathrm{i}k^{-2}\omega_{e\boldsymbol{k}}^2 \star \bar{\mathbf{B}}_{nv} - \mathrm{i}\bar{\boldsymbol{u}}^{\top} \star \bar{\mathbf{B}}_{vv} - \omega_{\mathrm{pe}}^{-1} \bar{\mathbf{W}}_{\psi v} \star \omega_{\boldsymbol{k}}^2.
\end{aligned}\right\} \tag{2.12}$$

Here $\omega_{\boldsymbol{k}}^2 = \omega_{\mathrm{pe}}^2 + k^2 c^2$ is the electromagnetic wave frequency. All of the $\mathbf{B}$ quantities are not of interest and simply facilitate the calculation; they are defined as follows: $\mathbf{B}_{nv} \doteq \mathbf{W}_{n\phi} - \mathbf{W}_{n\chi}$, $\mathbf{B}_{\psi v} \doteq \mathbf{W}_{\psi\phi} - \mathbf{W}_{\psi\chi}$, $\mathbf{B}_{vv} \doteq \mathbf{W}_{\phi\phi} + \mathbf{W}_{\chi\phi} - \mathbf{W}_{\phi\chi} - \mathbf{W}_{\chi\chi}$. Here, the fact that $\mathbf{W}_{vv} = \mathbf{W}_{\phi\phi} + \mathbf{W}_{\chi\phi} + \mathbf{W}_{\phi\chi} + \mathbf{W}_{\chi\chi}$ is used, which follows from the linearity of the Wigner transform.

The crucial step, which is the essence of the CE2 closure, is the splitting of the average of the product, into the product of the averages, for the third-order quantities: $\overline{\boldsymbol{\eta}^{\top} \star \mathbf{W}} = \bar{\boldsymbol{\eta}}^{\top} \star \bar{\mathbf{W}}$. This effectively assumes the third-order cumulant $\overline{\tilde{\boldsymbol{\eta}}^{\top} \star \tilde{\mathbf{W}}}$ to be negligible (the tilde denotes the fluctuating part of the quantity) (Krommes & Parker 2019). It is exactly zero for fields obeying jointly normal (Gaussian multivariate) statistics. In contrast to turbulence, here this assumption is easier to justify. One does not expect the interactions between the fluctuations to be of interest, which is what is being neglected when one discards higher-order cumulants and assumes Gaussianity. They would not be of interest since such effects are what leads to fluctuation intermittency, or are responsible for the typical turbulent energy cascades, neither of which is assumed here to be of relevance in the linear stage of the instability. The fluctuations in the electric field of the laser pulse are prescribed in a sense (their power spectrum $\bar{\mathbf{W}}_{vv}$ is given), and are expected to be normal for both temporally incoherent pulses (Goodman 2015), as well as transversely incoherent fields produced by a random phase plate for example (Rose & DuBois 1993; Garnier 1999), where in both cases this is a consequence of the central limit theorem. Hence the driving field $\boldsymbol{v}_{\mathrm{os}}$ is safely assumed a Gaussian random process. It should be noted that the Wigner–Moyal formalism is also very useful in deriving more sophisticated closures such as the quasi-normal one as shown by Ruiz *et al.* (2019).

The Wigner function is bilinear and therefore $\mathbf{B}_{vv} = \mathbf{W}_{(\phi+\chi)(\phi-\chi)}$. If the laser field $\boldsymbol{v}_{\mathrm{os}}$ is statistically stationary, it is shown in Appendix C that the ensemble-averaged Wigner function $\bar{\mathbf{W}}_{vv}$ and the associated quantity $\bar{\mathbf{B}}_{vv}$ are related as follows: $\bar{\mathbf{B}}_{vv}(\boldsymbol{k}) = \omega_{\mathrm{pe}}^{-1}\omega_{\boldsymbol{k}} \bar{\mathbf{W}}_{vv}(\boldsymbol{k})$. This is an important step in the derivation as it makes all symbol products in (2.12) have one of the quantities being a function of $\boldsymbol{x}$ or $\boldsymbol{k}$ only. Taking the Fourier transform of the system results in

$$\left.\begin{aligned}
-\Omega \mathring{\bar{\mathbf{W}}}_{nv} &= \mathrm{i}k_-^2 \mathring{\bar{\mathbf{W}}}_{\psi v} - \mathrm{i}\mathring{\bar{\boldsymbol{\eta}}}^{\top} \bar{\mathbf{W}}_{vv}^{+} - \omega_{\mathrm{pe}} \mathring{\bar{\mathbf{B}}}_{nv}, \\
-\Omega \mathring{\bar{\mathbf{B}}}_{nv} &= \mathrm{i}k_-^2 \mathring{\bar{\mathbf{B}}}_{\psi v} - \mathrm{i}\omega_{\mathrm{pe}}^{-1}\omega_{k_+} \mathring{\bar{\boldsymbol{\eta}}}^{\top} \bar{\mathbf{W}}_{vv}^{+} - \omega_{\mathrm{pe}}^{-1}\omega_{k_+}^2 \mathring{\bar{\mathbf{W}}}_{nv}, \\
-\Omega \mathring{\bar{\mathbf{W}}}_{\psi v} &= -\mathrm{i}k_-^{-2}\omega_{ek_-}^2 \mathring{\bar{\mathbf{W}}}_{nv} - \mathrm{i}\mathring{\bar{\boldsymbol{u}}}^{\top} \bar{\mathbf{W}}_{vv}^{+} - \omega_{\mathrm{pe}} \mathring{\bar{\mathbf{B}}}_{\psi v}, \\
-\Omega \mathring{\bar{\mathbf{B}}}_{\psi v} &= -\mathrm{i}k_-^{-2}\omega_{ek_-}^2 \mathring{\bar{\mathbf{B}}}_{nv} - \mathrm{i}\omega_{\mathrm{pe}}^{-1}\omega_{k_+} \mathring{\bar{\boldsymbol{u}}}^{\top} \bar{\mathbf{W}}_{vv}^{+} - \omega_{\mathrm{pe}}^{-1}\omega_{k_+}^2 \mathring{\bar{\mathbf{W}}}_{\psi v},
\end{aligned}\right\} \tag{2.13}$$

where the quantities with superscripts $\pm$ are evaluated at $\boldsymbol{k}_{\pm} = \boldsymbol{k} \pm \frac{1}{2}\boldsymbol{K}$, $\mathring{\bar{\boldsymbol{\eta}}}$ and $\mathring{\bar{\boldsymbol{u}}}$ are functions of $\boldsymbol{K}$ only (the Fourier image of $\boldsymbol{x}$) and all other quantities are functions of both $\boldsymbol{k}$ and $\boldsymbol{K}$.

https://doi.org/10.1017/S0022377824000953 Published online by Cambridge University Press

In order to keep the model self-consistent under the assumed ordering, the growth rate of the instability can be calculated only up to order $v_{\rm os}/c$ and higher-order terms need to be discarded (Kruer 2019). The way this works in the present case is as follows. To close the system (2.13), $\mathring{\boldsymbol{u}}$ can be expressed in terms of $\mathring{\eta}$ and $\mathring{\mathbf{W}}_{\psi v}$ through the second equation in the TPD system (2.2). Then the equations containing $\mathring{\boldsymbol{u}}$ will involve terms which are $\propto \mathring{\mathbf{W}}_{\psi v}\mathring{\mathbf{W}}_{vv}$. As in the standard derivation in Kruer (2019), this introduces terms of order $(v_{\rm os}/c)^2 \ll 1$ in the growth rate which are ignored, and therefore in (2.13) one uses the approximation $\mathring{\boldsymbol{u}} = \mathrm{i}(\Omega/K^2)\mathring{\boldsymbol{\eta}}$.

Solving the system for the quantities of interest, $\mathring{\bar{\mathbf{W}}}_{\psi v}$ and $\mathring{\bar{\mathbf{W}}}_{nv}$, in terms of the laser field $\bar{\mathbf{W}}_{vv}$ and substituting them into (2.7) results in the homogeneous broadband TPD dispersion relation:

$$D_e(\Omega, \boldsymbol{K}) = \int \frac{\mathrm{d}\boldsymbol{k}}{(2\pi)^3} \frac{(k_-^2\,\Omega - K^2\Omega_-)^2}{K^2 k_-^2 D_e(\Omega_-, \boldsymbol{k}_-)} \boldsymbol{k}_- \boldsymbol{K}^\top : \bar{\mathbf{W}}_{vv}(\boldsymbol{k}), \tag{2.14}$$

where $\Omega_- = \omega_{\boldsymbol{k}} - \Omega$, the integral is to be taken along the Landau contour, $\boldsymbol{k}_- \doteq \boldsymbol{k} - \boldsymbol{K}$ has been redefined and the colon denotes double matrix contraction.[3] This is the main result of the new model. For a statistically stationary random process, the two-point correlation function and the power spectrum form a Fourier pair (Wiener–Khinchin theorem) (Goodman 2015). So one can notice that the expression has a familiar form and a simple physical interpretation: the broadband dispersion relation is the monochromatic one integrated over the laser field power spectrum $\bar{\mathbf{W}}_{vv}(\boldsymbol{k})$, given by

$$\bar{\mathbf{W}}_{vv}(\boldsymbol{k}) = \int \mathrm{d}\boldsymbol{s}\, \mathrm{e}^{-\mathrm{i}\boldsymbol{k}\cdot\boldsymbol{s}} \overline{\boldsymbol{v}_{\rm os}(\boldsymbol{x} + \boldsymbol{s}/2)\boldsymbol{v}_{\rm os}^\dagger(\boldsymbol{x} - \boldsymbol{s}/2)}. \tag{2.15}$$

This dispersion relation allows one to study the homogeneous TPD under laser fields with arbitrary power spectra.

3. Applications

3.1. *Monochromatic beams*

The broadband TPD dispersion relation (2.14) reduces to the well-known result for a monochromatic plane wave. Consider a pump of the form $\boldsymbol{v}_{\rm os}(t, \boldsymbol{x}) = \frac{1}{2} v_{\rm os}\boldsymbol{\sigma}\, \mathrm{e}^{\mathrm{i}\boldsymbol{k}_0\cdot\boldsymbol{x} - \mathrm{i}\omega_0 t} +$ c.c., where $\omega_0 \equiv \omega_{\boldsymbol{k}_0}$ is the laser frequency and $\boldsymbol{\sigma}$ is the laser polarisation. The polarisation $\boldsymbol{\sigma}$ is allowed to be complex to take into account circularly polarised laser beams as well. The Wigner function of this field is[4]

$$\bar{\mathbf{W}}_{vv}(\boldsymbol{k}) = \tfrac{1}{4}(2\pi)^3 v_{\rm os}^2 [\boldsymbol{\sigma}\boldsymbol{\sigma}^\dagger \delta(\boldsymbol{k} - \boldsymbol{k}_0) + \boldsymbol{\sigma}^*\boldsymbol{\sigma}^\top \delta(\boldsymbol{k} + \boldsymbol{k}_0)]. \tag{3.1}$$

Substituting this in (2.14), and as usual ignoring the anti-Stokes term for being off-resonant, reduces to the familiar expression (see Kruer 2019):

$$D_e(\Omega, \boldsymbol{K}) D_e(\omega_0 - \Omega, \boldsymbol{K} - \boldsymbol{k}_0) = \frac{\omega_{\rm pe}^2 v_{\rm os}^2 |\boldsymbol{K}\cdot\boldsymbol{\sigma}\,|^2}{4} \left(\frac{K^2 - |\boldsymbol{K} - \boldsymbol{k}_0|^2}{K|\boldsymbol{K} - \boldsymbol{k}_0|} \right)^2, \tag{3.2}$$

[3] The double matrix contraction is defined as $\boldsymbol{A} : \boldsymbol{B} = \sum_{ij} A_{ij} B_{ji}$. For matrices which can be written as $\boldsymbol{A} = \boldsymbol{a}_1\boldsymbol{a}_2^\top$ and $\boldsymbol{B} = \boldsymbol{b}_1\boldsymbol{b}_2^\top$ one has $\boldsymbol{A} : \boldsymbol{B} = (\boldsymbol{a}_1\cdot\boldsymbol{b}_2)(\boldsymbol{a}_2\cdot\boldsymbol{b}_1)$.

[4] This is derived by assuming the wave has some random initial phase which is averaged over. This averaging is equivalent to the mode truncation procedure which appears in the usual derivation (Kruer 2019), in which the coupling of the laser to plasma oscillations at $\omega \pm 2\omega_0$, $\omega \pm 3\omega_0$ etc. is ignored. The validity of this approximation was studied by Machacek & Wark (2001). There is an exactly equivalent issue in the DW-ZF problem which concerns the modulational instability of a single drift-wave mode, and the derivation of the growth rate from the generalised zonostrophic instability dispersion relation. For details, see Parker (2014). Other kinds of averaging which produce the same result are also possible (Dodin 2022).

https://doi.org/10.1017/S0022377824000953 Published online by Cambridge University Press

where one has used the approximation $\Omega \simeq \Omega_- \simeq \omega_{\rm pe}$ in the numerator.

In the case of multiple monochromatic non-interfering laser beams, the Wigner function is (ignoring the anti-Stokes terms)

$$\bar{\mathbf{W}}_{vv}(\boldsymbol{k}) = \sum_i \tfrac{1}{4}(2\pi)^3 v_{{\rm os},i}^2 \boldsymbol{\sigma}_i \boldsymbol{\sigma}_i^\dagger \delta(\boldsymbol{k} - \boldsymbol{k}_{0i}). \tag{3.3}$$

The dispersion relation in this case becomes

$$D_e(\Omega, \boldsymbol{K}) = \sum_i \left| \frac{|\boldsymbol{K} - \boldsymbol{k}_{0i}|^2 - K^2}{2K|\boldsymbol{K} - \boldsymbol{k}_{0i}|} (\boldsymbol{K}\cdot\boldsymbol{\sigma}_i) v_{{\rm os},i} \right|^2 \frac{\omega_{\rm pe}^2}{D_e(\omega_0 - \Omega, \boldsymbol{K} - \boldsymbol{k}_{0i})}. \tag{3.4}$$

This agrees with the result of Michel *et al.* (2013).

3.2. *Single temporally incoherent beam*

Next, consider a single temporally incoherent laser beam. The Wigner function describing such a field is of the form (again ignoring the anti-Stokes term)

$$\bar{\mathbf{W}}_{vv}(\boldsymbol{k}) = \tfrac{1}{4}(2\pi)^3 v_{\rm os}^2 \boldsymbol{\sigma}\boldsymbol{\sigma}^\dagger G(k_\parallel)\delta(\boldsymbol{k}_\perp), \tag{3.5}$$

where $G(k_\parallel)$ is the power spectrum centred around k_0 and normalised such that it integrates to unity. Also, $k_\parallel \doteq \boldsymbol{k}\cdot\hat{\boldsymbol{\kappa}}$, $\boldsymbol{k}_\perp \doteq \boldsymbol{k} - k_\parallel\hat{\boldsymbol{\kappa}}$ with $\hat{\boldsymbol{\kappa}} \doteq \boldsymbol{k}_0/k_0$ being the unit vector in the direction of propagation. For $\Delta\omega/\omega_0 \ll 1$, the wavenumber spread Δk is related to the frequency bandwidth through $\Delta\omega = v_{g0}\Delta k$, where $v_{g0} = \partial\omega_{\boldsymbol{k}}/\partial k|_{k_0}$ is the group velocity of electromagnetic waves at the peak of the power spectrum. Most commonly one considers broadband lasers with top-hat (flat), Lorentzian or Gaussian power spectra (Follett *et al.* 2019). Upon substitution of (3.5) in (2.14), the dispersion relation has the form

$$D_e(\Omega, \boldsymbol{K}) = \frac{K_\perp^2 v_{\rm os}^2}{4}\mathscr{I}. \tag{3.6}$$

Here, in the same way as before $\boldsymbol{K}_\perp \doteq \boldsymbol{K} - \boldsymbol{K}\cdot\hat{\boldsymbol{\kappa}}$. The integral $\mathscr{I}$ is given by

$$\mathscr{I} = \int_{C_L} \frac{{\rm d}\omega_{k_\parallel}}{v_g(\omega_{k_\parallel})} \frac{\mathsf{C}(\omega_{k_\parallel})G(\omega_{k_\parallel})}{(\omega_{k_\parallel} - \Omega)^2 - \omega_{e\boldsymbol{k}_-}^2}, \tag{3.7}$$

in which the integration variables have been changed from $\boldsymbol{k}$ to $\omega_{\boldsymbol{k}}$ in order to deal with the pole in the integrand more easily; note that the integral should be taken along the Landau contour C_L. The function C has been defined as $\mathsf{C}(k_\parallel) \doteq (K^2\Omega_- - k_-^2\Omega)^2/(Kk_-)^2$. Note that C is a function of Ω and $\boldsymbol{K}$ as well, but those have been dropped for brevity. Of course here by k_- one means $k_- = |\boldsymbol{K} - k_\parallel\hat{\boldsymbol{\kappa}}|$. In order not to make the notation too cumbersome, functions such as C, the spectrum G, or $\omega_{e\boldsymbol{k}_-}$ which are defined as functions of $k_\parallel$, one evaluates in terms of the frequency implicitly as follows: $\mathsf{C}(\omega_{k_\parallel}) \equiv \mathsf{C}[\mathsf{K}(\omega_{k_\parallel})]$, where $\mathsf{K}(\omega_{\boldsymbol{k}}) \doteq c^{-1}\sqrt{\omega_{\boldsymbol{k}}^2 - \omega_{\rm pe}^2} = k$ allows one to go from the laser frequency to the laser wavenumber.

In the monochromatic case, the TPD growth rate maximises to a value of $\gamma_0 = \frac{1}{4}k_0 v_{\rm os}$. This tells one that $\gamma_0/\omega_{\rm pe} \ll 1$ since $\gamma_0/\omega_{\rm pe} \sim k_0 v_{\rm os}/\omega_{\rm pe} \sim v_{\rm os}/c \ll 1$. The right-hand side of (3.6) is of order $\gamma_0^2 \ll \omega_{\rm pe}^2$. Therefore it is possible to assume that the real part of the

https://doi.org/10.1017/S0022377824000953 Published online by Cambridge University Press

frequency satisfies the linear dispersion relation: $\Omega = \omega_{eK} + \mathrm{i}\gamma$. With this the growth rate becomes

$$\gamma = \frac{K_\perp^2 v_{\mathrm{os}}^2}{4} \frac{1}{2\omega_{eK}} \mathrm{Im}[\mathscr{I}], \tag{3.8}$$

and the integral $\mathscr{I}$ is

$$\mathscr{I} = \int_{C_L} \frac{\mathrm{d}\omega_{k_\parallel}}{v_g(\omega_{k_\parallel})} \frac{\mathsf{C}(\omega_{k_\parallel}) G(\omega_{k_\parallel})}{(\omega_{k_\parallel} - \omega_{eK} - \mathrm{i}\gamma - \omega_{e\boldsymbol{k}_-})(\omega_{k_\parallel} - \omega_{eK} - \mathrm{i}\gamma + \omega_{e\boldsymbol{k}_-})}. \tag{3.9}$$

The integrand of $\mathscr{I}$ has one pole of interest which occurs at a wavenumber $k_p(\boldsymbol{K})$ such that $\omega_{k_p} - \omega_{eK} - \omega_{e\boldsymbol{k}_-} = 0$. This is the frequency-matching condition which for a given k_p defines a circle in $\boldsymbol{K}$-space centred around $(K_\parallel, K_\perp) = (k_0/2, 0)$. In the limit of large bandwidth $\Delta\omega \gg \gamma$ one evaluates $\mathscr{I}$ using Plemelj's formula:

$$\lim_{\varepsilon \to 0^+} \int_{-\infty}^{\infty} \frac{f(x)}{x - \zeta \mp \mathrm{i}\varepsilon} \mathrm{d}x = \mathscr{P} \fint_{-\infty}^{\infty} \frac{f(x)}{x - \zeta} \mathrm{d}x \pm \mathrm{i}\pi f(\zeta), \tag{3.10}$$

with $\mathscr{P} \fint$ denoting the principal value integral and $\zeta, \varepsilon \in \mathbb{R}$. Physically this is due to the fact that for small growth rates, the resonance is very sharp and the instability is driven only by the part of the power spectrum which can perfectly satisfy the matching conditions. Evaluating the imaginary part at the pole:

$$\mathrm{Im}[\mathscr{I}] = \pi \frac{\mathsf{C}(k_p) G(k_p)}{v_g(k_p)(\omega_{k_p} - \omega_{eK} + \omega_{e\boldsymbol{k}_-})} \simeq \pi \frac{\mathsf{C}(k_p) G(k_p)}{v_{g0}\, \omega_0}. \tag{3.11}$$

This gives the growth rate of the TPD instability in a uniform plasma in the case of a single temporally incoherent laser beam:

$$\gamma_K = \frac{\pi G(k_p)}{v_{g0}} \gamma_{0\boldsymbol{K}}^2, \tag{3.12}$$

where one uses the fact that $(K_\perp^2 v_{\mathrm{os}}^2 / 8\omega_{eK}\omega_0)\mathsf{C}(k_p, \boldsymbol{K}) \simeq (K_\perp^2 v_{\mathrm{os}}^2/16)((K^2 - |\boldsymbol{K} - k_p\hat{\boldsymbol{\kappa}}|^2)^2 / K^2|\boldsymbol{K} - k_p\hat{\boldsymbol{\kappa}}|^2) = \gamma_{0\boldsymbol{K}}^2$, and γ_{0K} is the monochromatic growth rate. The reader is reminded here that the wavenumber at which the resonance occurs k_p is a function of $\boldsymbol{K}$ and is determined from the frequency-matching condition: $\omega_{k_p} - \omega_{eK} - \omega_{e\boldsymbol{k}_-} = 0$.

Consider next the maximum value that γ_K attains over all wavenumbers $\boldsymbol{K}$. Evaluating that for the top-hat and Lorentzian power spectra: for the top hat $G(k_0) = 1/\Delta k$ and so the growth rate is $\gamma_{\mathrm{TH}} = \pi\gamma_0^2/\Delta\omega$. For the Lorentzian $G(k) = (1/\pi)(\Delta k/2/((k - k_0)^2 + (\Delta k/2)^2))$ one has $G(k_0) = 2/\pi\Delta k$ and so $\gamma_L = 2\gamma_0^2/\Delta\omega$. Here $\gamma_0 = \frac{1}{4} k_0 v_{\mathrm{os}}$ is the value at which γ_{0K} maximises. These results agree with the well-known scaling of the growth rate as $\gamma \sim \gamma_0^2/\Delta\omega$, but also include the dependence of the result on the laser spectral shape. It is interesting to note that while the coherence times for the two power spectra are (for the top hat and Lorentzian, respectively) $\tau_c = 2\pi/\Delta\omega, 2/\Delta\omega$ (see also § 3.3 for a definition of τ_c) (Goodman 2015; Follett *et al.* 2019), the growth rates differ by less than a factor of π. This shows that at least in the homogeneous case, it is not the coherence time *per se* which is the most relevant metric, but rather the fraction of laser energy which satisfies the resonance conditions. At first glance this is somewhat at odds with the results of Follett *et al.* (2019), which found that the coherence time provides a universal scaling for the absolute Raman and TPD

https://doi.org/10.1017/S0022377824000953 Published online by Cambridge University Press

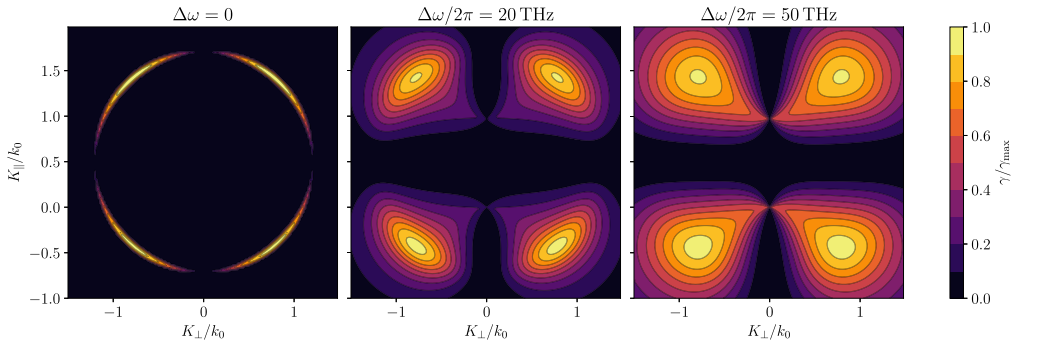

FIGURE 2. Effect of laser bandwidth on the range of unstable wavenumbers excited by the TPD instability as driven by a single broadband laser beam. The laser has a Lorentzian power spectrum, an intensity of $I_L = 10^{15}\,\mathrm{W\,cm^{-2}}$ and wavelength $\lambda = 350$ nm; the plasma conditions are $T_e = 2$ keV and $n_e = 0.23 n_c$ (n_c being the critical density). The growth rates are normalised to the maximal growth rate corresponding to each configuration. The left-hand panel represents the monochromatic case by solving (3.2) so it is normalised to $\gamma_{\max} = \gamma_0 = \frac{1}{4} k_0 v_{\mathrm{os}}$. The middle and right-hand panels show the analytical broadband solution $\gamma_{\boldsymbol{K}}$ and are thus normalised to $\gamma_{\max} = \gamma_L = 2\gamma_0^2/\Delta\omega$.

thresholds, meaning that the thresholds were the same for fields with the same coherence times but different spectral shapes. More formally, it appears that the peak growth rates of the instability scale with $G(k_0)$, and the absolute thresholds with $\int |G(k)|^2\,\mathrm{d}k$. The reason for this difference in behaviour is unknown but the problem of an absolute instability near the quarter critical density in an inhomogeneous plasma is significantly more complicated and there is little reason to expect that it should be affected by bandwidth in the same way as the temporal growth rate in a homogeneous plasma, which has been calculated here.

Having explored how bandwidth affects the maximum value the growth rate attains, one now turns to how it modifies the spectrum of excited plasma waves. First in the monochromatic case, plasma waves are driven at wavenumbers near the intersection of the circles defined by the frequency-matching condition, and the hyperbolas defined by $K_\perp^2 = K_\parallel(K_\parallel - k_0)$ at which the monochromatic growth rate $\gamma_{0\boldsymbol{K}}$ maximises. This is shown in the left-hand panel in figure 2. In the middle and right-hand panels the growth rate $\gamma_{\boldsymbol{K}}$ is presented, for a Lorentzian power spectrum of varying bandwidths. One sees that increasing the laser bandwidth significantly broadens the range of unstable wavenumbers excited by the TPD instability. In the right-hand panel virtually the entire TPD hyperbolas are observed since the ultra-large laser bandwidth allows all relevant wavenumbers to satisfy the frequency-matching conditions. What is most interesting is that even for relatively modest amounts of bandwidth such as 20 THz (middle panel) the broadening of the spectrum is substantial. Such effects may change the nature of the instability. For example, in an inhomogeneous plasma, at lower densities the TPD modes are fairly high in $\boldsymbol{K}$ as illustrated by the left-hand panel in figure 2, and tend to be convective. Absolute modes occur near $|\boldsymbol{K}| \to 0$, which would typically be excited only in regions very close to the quarter critical density (Yan, Maximov & Ren 2010). One sees that laser bandwidth favours the absolute instability at lower densities too.

The analytical results presented so far have relied upon the assumption that the bandwidth is large compared with the growth rate $\Delta\omega \gg \gamma_0$, which was used in the evaluation of the integral $\mathscr{I}$ in (3.9). To explore the growth rates of the instability in the intermediate regime $\Delta\omega \sim \gamma_0$, the integral is evaluated numerically for finite γ. Figure 3 shows the growth rate calculated along the lower branch of the TPD hyperbolas as a

https://doi.org/10.1017/S0022377824000953 Published online by Cambridge University Press

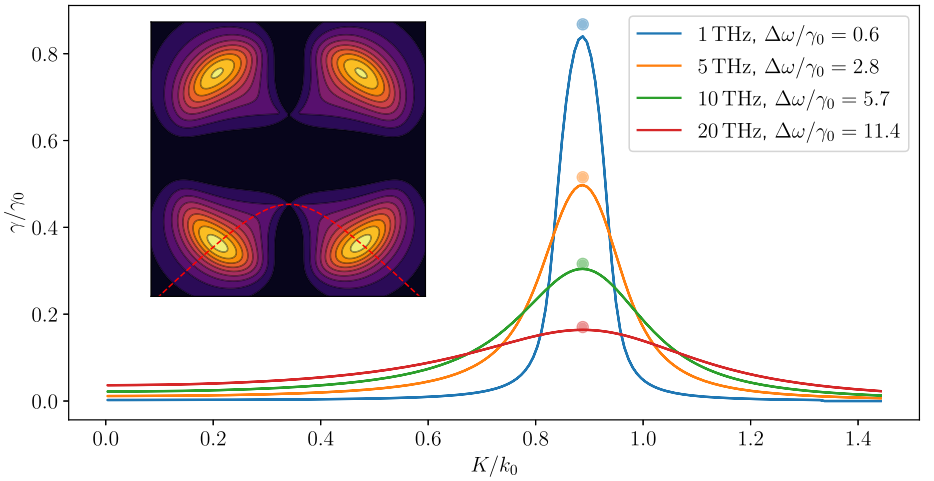

FIGURE 3. Numerically evaluated growth rates γ in the intermediate-bandwidth regime calculated along the lower branch of the TPD hyperbolas defined by $K_\perp^2 = K_\parallel(K_\parallel - k_0)$. The inset shows the middle panel of figure 2 along with the aforementioned hyperbola as represented by the red dashed line. The plasma conditions and laser parameters are the same as those described in figure 2. The growth rate is normalised to the monochromatic one γ_0, and the horizontal axis represents the magnitude of the wavenumber $K = \sqrt{K_\parallel^2 + K_\perp^2}$. The circles represent the estimate of the maximum growth rate as given by (3.14).

function of the magnitude of the wavenumber K. One sees that even at the fairly low bandwidth of 5 THz ($\Delta\omega/\gamma_0 = 2.8$) and at intensity $I_L = 10^{15}\,\mathrm{W\,cm^{-2}}$, the growth rate is half its monochromatic value. It is also approximately a third for $\Delta\omega/2\pi = 10$THz (corresponding to the intrinsic bandwidth of an argon fluoride laser). As shown below, laser wavelength does not affect the peak values of the growth rate and therefore the results just quoted are unchanged by it. Decreasing the wavelength though does reduce the broadening effect in the plasma wave spectrum shown in figure 2.

In addition, it is possible to calculate the peak of the growth rates analytically in this regime. This is done by ignoring the thermal correction in the dispersion functions and assuming the wavenumber $\boldsymbol{K}$ is along the TPD hyperbola, leading to an expression for the maximum growth rate of the form

$$\gamma_{\max} = \gamma_0^2 \int \frac{2\omega_{\mathrm{pe}}\, G(\omega_{k_\parallel})}{(\omega_{k_\parallel} - 2\omega_{\mathrm{pe}} - \mathrm{i}\gamma_{\max})(\omega_{k_\parallel} - \mathrm{i}\gamma_{\max})}\, \mathrm{d}\omega_{k_\parallel}. \tag{3.13}$$

For a Lorentzian spectrum centred at $\omega_0 = 2\omega_{\mathrm{pe}}$ the integral can be evaluated exactly, leading to

$$\gamma_{\max} = \tfrac{1}{4}(\sqrt{16\gamma_0^2 + \Delta\omega^2} - \Delta\omega). \tag{3.14}$$

This reproduces the two relevant limits: for $\Delta\omega \to 0$, $\gamma_{\max} \to \gamma_0$; and for $\Delta\omega \to \infty$, $\gamma_{\max} \to \gamma_L = 2\gamma_0^2/\Delta\omega$. Since γ_0 does not depend on laser wavelength, then $\gamma_{\max}$ does not either. The circles in figure 3 represent $\gamma_{\max}$ as given by the result above, showing excellent agreement with the numerically calculated growth rate.

https://doi.org/10.1017/S0022377824000953 Published online by Cambridge University Press

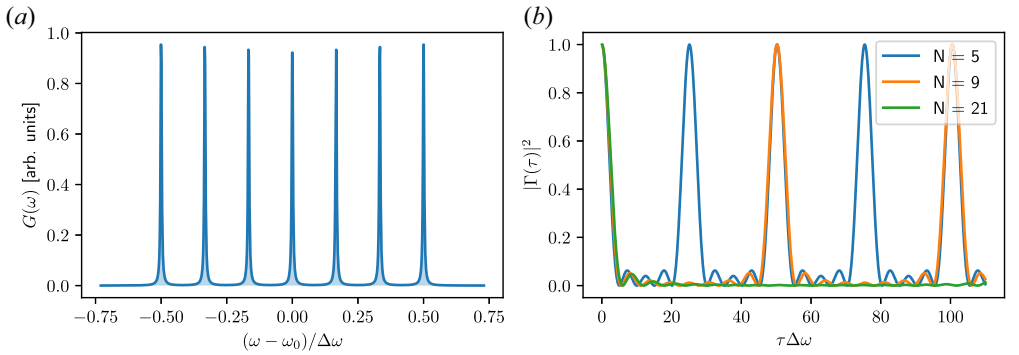

FIGURE 4. (*a*) A power spectrum $G(\omega)$ consisting of $N = 7$ well-separated spectral lines, centred around ω_0 and spread over a bandwidth of $\Delta\omega$. Their thickness is finite for the purposes of visualisation. (*b*) The normalised correlation function $|\Gamma(\tau)|^2$ as a function of the time separation τ of a set of N delta-shaped spectral lines spread over a bandwidth $\Delta\omega$.

3.3. *Well-separated discrete spectral lines*

Another implication concerns the extent to which a power spectrum consisting of N well-separated sharp spectral lines spread over a bandwidth $\Delta\omega$, such as that shown in figure 4(*a*), approximates the instability reduction properties of a continuous power spectrum (Bodner 2023). For sufficiently low number of spectral lines, such that only a single line is contained within the instability resonance, $\Delta\omega/(N-1) > \gamma_0$, following the generalised dispersion relation presented here, the instability growth rate will be $\gamma = \gamma_0/\sqrt{N}$. From the aforementioned inequality, this reduction will be somewhat lower than the expected $\pi\gamma_0^2/\Delta\omega$ in the continuous case, but still significant. For example for $N = 10$, the reduction is similar to that of 10 THz continuous bandwidth (see figure 3). At first glance this reduction cannot be explained by the coherence properties of the power spectrum, since formally if each line is delta-shaped, the coherence time is infinite.

To investigate this, one follows Goodman (2015). Consider a power spectrum containing N discrete delta-shaped spectral lines, uniformly spread over a bandwidth of $\Delta\omega$, and centred around ω_0 (figure 4*a*):

$$G(\omega) = \frac{1}{N}\sum_{j=0}^{N-1}\delta\left(\omega - \omega_0 - \frac{\Delta\omega}{2} + \frac{\Delta\omega}{N-1}j\right). \tag{3.15}$$

This is the power spectrum of the complex analytic signal $Y(t)$ where the actual signal is $y(t) = \mathrm{Re}Y(t)$. By the Wiener–Khinchin theorem, the correlation function $C(\tau) = \overline{Y^*(t)Y(t+\tau)}$ is given by the (inverse) Fourier transform of $G(\omega)$:

$$C(\tau) = \frac{1}{2\pi}\int G(\omega)\,\mathrm{e}^{-\mathrm{i}\omega t}\,\mathrm{d}t. \tag{3.16}$$

Defining the normalised correlation function $\Gamma(\tau) = C(\tau)/C(0)$, the coherence time for a random process is given by

$$\tau_c = \int_{-\infty}^{\infty}|\Gamma(\tau)|^2\,\mathrm{d}\tau. \tag{3.17}$$

https://doi.org/10.1017/S0022377824000953 Published online by Cambridge University Press

It can be shown that the correlation function for the discrete power spectrum $G(\omega)$ is

$$|\Gamma(\tau)|^2 = \frac{1}{N^2}\csc^2\left(\frac{\Delta\omega\tau}{2(N-1)}\right)\sin^2\left(\frac{N\Delta\omega\tau}{2(N-1)}\right). \tag{3.18}$$

Formally, the integral of this will always diverge for any finite N. In the limit of $N \to \infty$ one recovers the normalised correlation function for a continuous top hat spectrum which has a finite coherence time:

$$|\Gamma_{\mathrm{TH}}(\tau)|^2 = \mathrm{sinc}^2(\Delta\omega\tau/2). \tag{3.19}$$

Figure 4(*b*) shows what $|\Gamma(\tau)|^2$ looks like for different numbers of spectral lines. One sees that for small τ the correlation functions closely resemble the sinc profile expected in the continuous case. In contrast, the discrete case exhibits correlations for larger τ, and the time scale over which these correlations occur increases with the number of spectral lines N. The kth peak occurs at time delay $T_k = 2(N-1)\pi k/\Delta\omega$. If T_1, the time at which the first peak occurs, is much larger than the typical time scale of interest (such as γ_0^{-1}) then the coherence properties of the continuous spectrum are well approximated by the discrete one. Using $T_1 \gg \gamma_0^{-1}$ translates to a condition on the number of spectral lines:

$$N \gg \frac{1}{2\pi}\frac{\Delta\omega}{\gamma_0}. \tag{3.20}$$

For a laser intensity of 10^{15} W cm^{-2} at a wavelength of 350nm and bandwidth of $\Delta\omega/\omega_0 =$ 1 %, the right-hand side is $\simeq$1. This suggests that even a low number of discrete spectral lines such as $N = 10$ might be a good approximation to the coherence properties of the continuous spectrum, as far as their effect on the instability is concerned.

4. Summary

In this paper, a novel statistical theory of the broadband TPD instability has been presented. It has been used to derive a dispersion relation in uniform plasma that is valid under laser electromagnetic fields with arbitrary power spectra. To achieve this, recent developments in inhomogeneous turbulence have been applied in order to derive the statistical closure required to treat the problem. The new dispersion relation is then applied to the study of the instability in a few cases of interest. For a single temporally incoherent laser beam, in the limit of large bandwidth $\Delta\omega \gg \gamma_0$, the well-known reduction of the peak of the growth rate by a factor of approximately $\gamma_0/\Delta\omega$ is confirmed, but it is also shown that the exact amount depends on the shape of the power spectrum. Namely, for a Lorentzian power spectrum the peak growth rate is $\gamma_L = 2\gamma_0^2/\Delta\omega$, and for a flat (top-hat) spectrum it is $\gamma_{\mathrm{TH}} = \pi\gamma_0^2/\Delta\omega$. This difference is less than what the difference in the coherence times of the two laser beams would imply. In addition, it has been shown that the laser bandwidth significantly broadens the range of wavenumbers excited by TPD. This implies that bandwidth favours the absolute instability in regions further away from the quarter critical density by allowing the $|\boldsymbol{K}| \to 0$ modes to be excited there too. The intermediate-bandwidth regime is explored numerically and it is shown that the growth rate is reduced to half its value for laser intensities of 10^{15} W cm^{-2} and relatively modest bandwidths of 5 THz. A power spectrum consisting of N discrete lines spread over a bandwidth of $\Delta\omega$ is also studied. It is shown that for a low number of spectral lines, the reduction in the peak growth rate is $1/\sqrt{N}$, which is somewhat smaller than in the continuous case but still significant.

https://doi.org/10.1017/S0022377824000953 Published online by Cambridge University Press

There some natural questions which arise as a consequence of this work. Firstly, can one model transversely incoherent laser fields such as those produced by a random phase plate (RPP), or a combination of transverse and temporal incoherence such as when a phase plate is combined with smoothing by spectral dispersion (SSD), as well as in the induced spatial coherence (ISI) scheme? Formally transverse incoherence can be straightforwardly incorporated by simply allowing the Wigner function (equivalently, the laser power spectrum) to have some finite angular spread in wavenumber. But since two laser fields which can have the same power spectrum can nonetheless still be very different, care should be taken when applying the generalised dispersion relation. The RPP field is such that it creates a speckle pattern at the focus which may cause the instability to be strongly localised within speckles with many times the average intensity (Follett *et al.* 2022). Such intermittent behaviour may break the Gaussianity assumption made in this work. Adding temporal incoherence by SSD or by using naturally broad-bandwidth lasers such as the excimer ones used in the ISI scheme causes the speckle pattern to move which may help smooth out this behaviour.

Secondly, the presence of a density gradient is primarily responsible for determining whether the dominant instability at the quarter critical density is the TPD or Raman scattering, with longer, ignition-relevant scale lengths favouring the Raman instability (Rosenberg *et al.* 2018). Therefore extending the present analysis to study the effects of laser bandwidth on the absolute instability in the presence of a density gradient is an important problem. The approach of Liu & Rosenbluth (1976) and Simon *et al.* (1983) for a plane-wave laser field uses some rather specific mathematical manipulations to calculate the absolute threshold, for which it is not immediately clear how they might be carried out within the framework presented in this paper. So this remains an interesting open problem.

Acknowledgements

The authors acknowledge useful discussions with Dr R. Follett and Dr J. Palastro (Laboratory for Laser Energetics, University of Rochester), Dr S. Bodner (Naval Research Laboratory – Emeritus) and Dr A. Bott (Oxford), as well as the two anonymous referees for their valuable input.

Editor Alex Schekochihin thanks the referees for their advice in evaluating this article.

Funding

R.T.R. was supported by the Saven European Scholarship and UKRI-EPSRC. R.A. was supported by the Oxford-ShanghaiTech collaboration agreement. The research was conducted under UKRI grants EP/X035336/1 and ST/V001655/1.

Declaration of interest

The authors report no conflict of interest.

Appendix A. The Weyl symbol calculus

Here a very brief introduction to the Weyl symbol calculus is provided. Although quite concise, this should give the reader most of the necessary background to understand the results in this paper. For details and proofs, see McDonald (1988), Tracy *et al.* (2014) and Dodin (2022) and references therein.

The symbol calculus is best presented in terms of abstract bra-kets and abstract operators acting on them. Therefore for any fields which might be of interest – the plasma density perturbation n, the velocity potential ψ, the quiver velocity $\boldsymbol{v}_{\mathrm{os}}$, etc. – one considers their abstract bra-ket representations. So for example, the position representation of the density

https://doi.org/10.1017/S0022377824000953 Published online by Cambridge University Press

perturbation is $n(\boldsymbol{x}) = \langle \boldsymbol{x} | n \rangle$; its Fourier transform, i.e. its wavenumber representation, is $\mathring{n}(\boldsymbol{k}) = \langle \boldsymbol{k} | n \rangle$.

One starts by defining the Wigner transform $\mathscr{W}$ of an abstract operator $\hat{A}$ as follows:

$$\mathsf{A}(\boldsymbol{x}, \boldsymbol{k}) \doteq \mathscr{W}[\hat{A}] \doteq \int \mathrm{d}\boldsymbol{s}\, \mathrm{e}^{-\mathrm{i}\boldsymbol{k}\cdot\boldsymbol{s}} \langle \boldsymbol{x} + \boldsymbol{s}/2 | \hat{A} | \boldsymbol{x} - \boldsymbol{s}/2 \rangle , \tag{A1}$$

where $\mathsf{A}(\boldsymbol{x}, \boldsymbol{k})$ is called the Weyl symbol of the operator $\hat{A}$. There is a close connection between the Wigner transform and correlation functions. The Wigner function of some field $\psi(\boldsymbol{x})$ is defined as

$$\mathsf{W}_{\psi\psi}(\boldsymbol{x}, \boldsymbol{k}) \doteq \int \mathrm{d}\boldsymbol{s}\, \mathrm{e}^{-\mathrm{i}\boldsymbol{k}\cdot\boldsymbol{s}} \psi(\boldsymbol{x} + \boldsymbol{s}/2) \psi^{\dagger}(\boldsymbol{x} - \boldsymbol{s}/2), \tag{A2}$$

where, from the definition, it is apparent that it can be thought of as the Fourier transform of the two-point correlation function of ψ (modulo some averaging procedure). The Wigner function is the symbol of the density operator $\hat{\rho} \doteq |\psi\rangle \langle\psi|$:

$$\mathsf{W}_{\psi\psi}(\boldsymbol{x}, \boldsymbol{k}) = \mathscr{W}[\hat{\rho}]. \tag{A3}$$

Analogously, one describes correlations between two different fields ψ and ϕ by considering the Wigner transform of $|\psi\rangle \langle\phi|$:

$$\mathsf{W}_{\psi\phi}(\boldsymbol{x}, \boldsymbol{k}) = \mathscr{W}[|\psi\rangle \langle\phi|] = \int \mathrm{d}\boldsymbol{s}\, \mathrm{e}^{-\mathrm{i}\boldsymbol{k}\cdot\boldsymbol{s}} \psi(\boldsymbol{x} + \boldsymbol{s}/2) \phi^{\dagger}(\boldsymbol{x} - \boldsymbol{s}/2). \tag{A4}$$

The Wigner transform possesses some nice properties:

$$\mathscr{W}[\mathbb{1}] = 1, \quad \mathscr{W}[\hat{x}_j^n] = x_j^n, \quad \mathscr{W}[\hat{k}_j^n] = k_j^n, \tag{A5a–c}$$

for any integer n, where $\mathbb{1}$ is the identity operator, $\hat{\boldsymbol{x}}$ is the abstract position operator with $\hat{x}_j$ being its jth component; analogously for the wavenumber operator $\hat{\boldsymbol{k}}$, which is the abstract representation of $-\mathrm{i}\partial_x$.[5] As a consequence, any reasonably behaved function F of those operators satisfies

$$\mathscr{W}[F(\hat{\boldsymbol{x}})] = F(\boldsymbol{x}), \quad \mathscr{W}[F(\hat{\boldsymbol{k}})] = F(\boldsymbol{k}). \tag{A6a,b}$$

This property makes it particularly easy to go from equations in the position representation as they are most commonly given to their abstract representation which is suitable for applying the Weyl symbol calculus. In the present work, this step does not even need be made explicit.

The symbol of a product of operators $\mathscr{W}[\hat{A}\hat{B}]$ is related to the individual symbols $\mathscr{W}[\hat{A}] = \mathsf{A}(\boldsymbol{x}, \boldsymbol{k})$ and $\mathscr{W}[\hat{B}] = \mathsf{B}(\boldsymbol{x}, \boldsymbol{k})$ through the Moyal star product $\star$ as follows:

$$\mathscr{W}[\hat{A}\hat{B}] = \mathsf{A}(\boldsymbol{x}, \boldsymbol{k}) \star \mathsf{B}(\boldsymbol{x}, \boldsymbol{k}), \tag{A7}$$

where the star product between two symbols is defined as

$$\mathsf{A}(\boldsymbol{x}, \boldsymbol{k}) \star \mathsf{B}(\boldsymbol{x}, \boldsymbol{k}) \doteq \mathsf{A}(\boldsymbol{x}, \boldsymbol{k})\, \mathrm{e}^{\mathrm{i}\hat{\mathcal{P}}/2} \mathsf{B}(\boldsymbol{x}, \boldsymbol{k}), \quad \hat{\mathcal{P}} = \overleftarrow{\partial}_{\boldsymbol{x}} \cdot \overrightarrow{\partial}_{\boldsymbol{k}} - \overleftarrow{\partial}_{\boldsymbol{k}} \cdot \overrightarrow{\partial}_{\boldsymbol{x}} \tag{A8a,b}$$

with $\hat{\mathcal{P}}$ being the Poisson bracket, and the arrows over the derivatives denoting the direction in which they act; $\mathsf{A}\hat{\mathcal{P}}\mathsf{B}$ represents the Poisson bracket between A and B. The

[5] This shows how similarly to Fourier transforms, when taking the Wigner transform of an equation, derivatives can be simply substituted for $\mathrm{i}\boldsymbol{k}$.

https://doi.org/10.1017/S0022377824000953 Published online by Cambridge University Press

symbol product and the Wigner transform are related to each other like the convolution and the Fourier transform.

Frequently one needs to calculate symbol products where one of the symbols is only a function of space, or only a function of wavenumber. In such cases, the symbol product simplifies greatly when Fourier transformed. Denoting the Fourier transform of $\psi(\boldsymbol{x})$ as $\mathring{\psi}(\boldsymbol{k}) \doteq \mathscr{F}_K[\psi(\boldsymbol{x})] = \int \mathrm{d}\boldsymbol{x}\, \psi(\boldsymbol{x})\, \mathrm{e}^{-\mathrm{i}\boldsymbol{K}\cdot\boldsymbol{x}}$, one has

$$\left.\begin{aligned} \mathscr{F}_K[F(\boldsymbol{k}) \star W(\boldsymbol{x},\boldsymbol{k})] &= F(\boldsymbol{k} - \tfrac{1}{2}\boldsymbol{K})\mathring{W}(\boldsymbol{K},\boldsymbol{k}), \\ \mathscr{F}_K[W(\boldsymbol{x},\boldsymbol{k}) \star F(\boldsymbol{k})] &= F(\boldsymbol{k} + \tfrac{1}{2}\boldsymbol{K})\mathring{W}(\boldsymbol{K},\boldsymbol{k}), \\ \mathscr{F}_K[G(\boldsymbol{x}) \star W(\boldsymbol{k})] &= \mathring{G}(\boldsymbol{K})W(\boldsymbol{k} + \tfrac{1}{2}\boldsymbol{K}), \end{aligned}\right\} \tag{A8}$$

for some generic functions F, G and W. The proof of the first one is as follows:

$$\begin{aligned} \mathscr{F}_K[F(\boldsymbol{k}) \star W(\boldsymbol{x},\boldsymbol{k})] &= \mathscr{F}_K\left[F(\boldsymbol{k}) \exp\left(\frac{\mathrm{i}\overleftarrow{\partial}_{\boldsymbol{x}}\cdot\overrightarrow{\partial}_{\boldsymbol{k}} - \mathrm{i}\overleftarrow{\partial}_{\boldsymbol{k}}\cdot\overrightarrow{\partial}_{\boldsymbol{x}}}{2}\right) W(\boldsymbol{x},\boldsymbol{k})\right] \\ &= F(\boldsymbol{k})\mathscr{F}_K\left[\exp\left(-\frac{1}{2}\mathrm{i}\overleftarrow{\partial}_{\boldsymbol{k}}\cdot\overrightarrow{\partial}_{\boldsymbol{x}}\right) W(\boldsymbol{x},\boldsymbol{k})\right] \\ &= F(\boldsymbol{k}) \exp\left(-\frac{1}{2}\overleftarrow{\partial}_{\boldsymbol{k}}\cdot\boldsymbol{K}\right) \mathring{W}(\boldsymbol{K},\boldsymbol{k}) \\ &= F\left(\boldsymbol{k} - \frac{1}{2}\boldsymbol{K}\right)\mathring{W}(\boldsymbol{K},\boldsymbol{k}). \end{aligned} \tag{A9}$$

The rest follow analogously.

For some field $|\psi\rangle$ governed by a Schrödinger-like equation $\mathrm{i}\partial_t|\psi\rangle = \hat{H}|\psi\rangle$ the density operator satisfies the von-Neumann equation:

$$\mathrm{i}\partial_t\hat{\rho} = \hat{H}\hat{\rho} - \hat{\rho}\hat{H}^\dagger. \tag{A10}$$

Taking the Wigner transform of the above gives the so-called Wigner–Moyal equation which governs the Wigner function of the field:

$$\mathrm{i}\partial_t \mathsf{W}_{\psi\psi} = \mathsf{H} \star \mathsf{W}_{\psi\psi} - \mathsf{W}_{\psi\psi} \star \mathsf{H}^\dagger, \tag{WME}$$

with $\mathsf{H} \doteq \mathscr{W}[\hat{H}]$ being the symbol of the Hamiltonian operator $\hat{H}$. This is what allows us to very efficiently go from the equations of motion (EOM) of some field ψ to the equation governing the correlation function of that field:

$$\text{EOM of } \psi \xrightarrow{\text{Weyl symbol calculus}} \text{EOM of the correlation function of } \psi. \tag{A11}$$

All of the above properties are also satisfied for vector fields $\boldsymbol{\Psi} = (\psi_1, \psi_2, \ldots)$ and matrices of operators $\hat{\boldsymbol{A}}$ as long as the usual matrix multiplication rules are respected. For example,

$$(\mathbf{A} \star \mathbf{B})_{ij} = \sum_k (\mathbf{A})_{ik} \star (\mathbf{B})_{kj}, \tag{A12}$$

where $\mathbf{A}$ and $\mathbf{B}$ are arbitrary matrix symbols. In this work, matrix multiplication rules are implied between symbols.

https://doi.org/10.1017/S0022377824000953 Published online by Cambridge University Press

Appendix B. The driving terms

Here a calculation identical to the one in Tsiolis *et al.* (2020) is reproduced which gives the form of the TPD driving terms. Consider the following:

$$\begin{aligned}\boldsymbol{v}_{\rm os}\cdot\nabla\psi &= \sum_j \mathrm{i}\,\langle \boldsymbol{x}|\,\hat{k}_j\,|\psi\rangle\,\langle \boldsymbol{x}\mid v_{{\rm os};j}\rangle \\ &= \sum_j \mathrm{i}\,\langle \boldsymbol{x}|\,\hat{k}_j\,|\psi\rangle\,\langle v_{{\rm os};j}\mid \boldsymbol{x}\rangle \\ &= \mathrm{i}\,\langle \boldsymbol{x}|\,\hat{\boldsymbol{k}}\cdot\hat{\boldsymbol{W}}_{\psi \boldsymbol{v}}\,|\boldsymbol{x}\rangle\,. \end{aligned} \tag{B1}$$

Here $\hat{\boldsymbol{W}}_{\psi \boldsymbol{v}} \doteq |\psi\rangle\,\langle \boldsymbol{v}_{\rm os}|$. So one sees that the expression $\boldsymbol{v}_{\rm os}\cdot\nabla\psi$ can be thought of as the matrix elements of the operator $\mathrm{i}\hat{\boldsymbol{k}}\cdot\hat{\boldsymbol{W}}_{\psi \boldsymbol{v}}$. For a general operator $\hat{A}$, it can be shown that these matrix elements can be related to the Weyl symbol $\mathsf{A}(\boldsymbol{x}, \boldsymbol{k})$ of the operator as follows (Dodin 2022):

$$\langle \boldsymbol{x}|\,\hat{A}\,|\boldsymbol{x}\rangle = \frac{1}{(2\pi)^3}\int \mathrm{d}\boldsymbol{k}\,\mathsf{A}(\boldsymbol{x}, \boldsymbol{k}). \tag{B2}$$

Hence using the Moyal star product, one writes

$$\boldsymbol{v}_{\rm os}\cdot\nabla\psi = \mathrm{i}\int \frac{\mathrm{d}\boldsymbol{k}}{(2\pi)^3}\boldsymbol{k}^{\top}\star \mathbf{W}^{\top}_{\psi \boldsymbol{v}}, \tag{B3}$$

since

$$\mathscr{W}[\hat{\boldsymbol{k}}\cdot\hat{\boldsymbol{W}}_{\psi \boldsymbol{v}}] = \boldsymbol{k}^{\top}\star \mathbf{W}^{\top}_{\psi \boldsymbol{v}}. \tag{B4}$$

Note that the transpose is needed in order for the dot product to be taken into account in the symbol product since $\boldsymbol{k}$ is a column vector and $\mathbf{W}_{\psi \boldsymbol{v}}$ is a row vector.

Appendix C. Proof of the relationship between $\mathbf{B}_{\boldsymbol{v}\boldsymbol{v}} \doteq \mathbf{W}_{(\boldsymbol{\phi}+\boldsymbol{\chi})(\boldsymbol{\phi}-\boldsymbol{\chi})}$ and $\mathbf{W}_{\boldsymbol{v}\boldsymbol{v}} = \mathbf{W}_{(\boldsymbol{\phi}+\boldsymbol{\chi})(\boldsymbol{\phi}+\boldsymbol{\chi})}$

The solution of the Klein–Gordon equation for the vector potential in a uniform plasma is of the form

$$\boldsymbol{A}(t, \boldsymbol{x}) = \int \frac{\mathrm{d}\boldsymbol{k}}{(2\pi)^3}\mathring{\boldsymbol{A}}(\boldsymbol{k})\,\mathrm{e}^{-\mathrm{i}\omega_{\boldsymbol{k}}t+\mathrm{i}\boldsymbol{k}\cdot\boldsymbol{x}}, \tag{C1}$$

with $\omega_{\boldsymbol{k}} = \sqrt{\omega_{\rm pe}^2 + k^2c^2}$ being the photon frequency. To calculate $\mathbf{B}_{\boldsymbol{v}\boldsymbol{v}}$ one needs $\partial_t\boldsymbol{v}_{\rm os}$ which is given by

$$\partial_t\boldsymbol{v}_{\rm os} = \int \frac{\mathrm{d}\boldsymbol{k}}{(2\pi)^3}(-\mathrm{i}\omega_{\boldsymbol{k}})\mathring{\boldsymbol{v}}_{\rm os}(\boldsymbol{k})\,\mathrm{e}^{-\mathrm{i}\omega_{\boldsymbol{k}}t+\mathrm{i}\boldsymbol{k}\cdot\boldsymbol{x}}. \tag{C2}$$

Let $\mathring{V}$ denote the Fourier transform of $\partial_t\boldsymbol{v}_{\rm os}$:

$$\mathring{V}(\boldsymbol{k}) \doteq \mathscr{F}_{\boldsymbol{k}}[\partial_t\boldsymbol{v}_{\rm os}] = -\mathrm{i}\omega_{\boldsymbol{k}}\mathring{\boldsymbol{v}}_{\rm os}(\boldsymbol{k}). \tag{C3}$$

It is straightforward to show that the Wigner function can be expressed in terms of the Fourier transforms of the fields as follows:

$$\mathsf{W}_{\psi\phi}(\boldsymbol{x}, \boldsymbol{k}) = \int \mathrm{d}\boldsymbol{k}'\,\mathrm{e}^{\mathrm{i}\boldsymbol{k}'\cdot\boldsymbol{x}}\mathring{\psi}(\boldsymbol{k}+\boldsymbol{k}'/2)\mathring{\phi}^{\dagger}(\boldsymbol{k}-\boldsymbol{k}'/2). \tag{C4}$$

https://doi.org/10.1017/S0022377824000953 Published online by Cambridge University Press

Therefore,

$$\mathbf{B}_{\boldsymbol{vv}} = \mathrm{i}\omega_{\mathrm{pe}}^{-1} \int \mathrm{d}\boldsymbol{k}'\, \mathrm{e}^{\mathrm{i}\boldsymbol{k}'\cdot\boldsymbol{x}} \mathring{\boldsymbol{v}}_{\mathrm{os}}(\boldsymbol{k}+\boldsymbol{k}'/2)\mathring{\boldsymbol{V}}^{\dagger}(\boldsymbol{k}-\boldsymbol{k}'/2)$$
$$= \omega_{\mathrm{pe}}^{-1} \int \mathrm{d}\boldsymbol{k}'\, \mathrm{e}^{\mathrm{i}\boldsymbol{k}'\cdot\boldsymbol{x}} \omega_{\boldsymbol{k}-\boldsymbol{k}'/2} \mathring{\boldsymbol{v}}_{\mathrm{os}}(\boldsymbol{k}+\boldsymbol{k}'/2)\mathring{\boldsymbol{v}}_{\mathrm{os}}^{\dagger}(\boldsymbol{k}-\boldsymbol{k}'/2). \tag{C5}$$

The equivalent expression for $\mathbf{W}_{\boldsymbol{vv}}$ is

$$\mathbf{W}_{\boldsymbol{vv}} = \int \mathrm{d}\boldsymbol{k}'\, \mathrm{e}^{\mathrm{i}\boldsymbol{k}'\cdot\boldsymbol{x}}\, \mathring{\boldsymbol{v}}_{\mathrm{os}}(\boldsymbol{k}+\boldsymbol{k}'/2)\mathring{\boldsymbol{v}}_{\mathrm{os}}^{\dagger}(\boldsymbol{k}-\boldsymbol{k}'/2). \tag{C6}$$

For spatially homogeneous fields, upon statistical averaging these wavenumber correlators will turn out to be deltas. To see that consider

$$\overline{\boldsymbol{a}(\boldsymbol{x}+\boldsymbol{s}/2)\boldsymbol{a}^{\dagger}(\boldsymbol{x}-\boldsymbol{s}/2)} = \int \mathrm{d}\boldsymbol{k}_1\mathrm{d}\boldsymbol{k}_2\, \overline{\mathring{\boldsymbol{a}}(\boldsymbol{k}_2)\mathring{\boldsymbol{a}}^{\dagger}(\boldsymbol{k}_1)}\, \mathrm{e}^{\mathrm{i}\boldsymbol{k}_1\cdot(\boldsymbol{x}-\boldsymbol{s}/2)}\, \mathrm{e}^{-\mathrm{i}\boldsymbol{k}_2\cdot(\boldsymbol{x}+\boldsymbol{s}/2)}$$
$$= \int \mathrm{d}\boldsymbol{k}_1\mathrm{d}\boldsymbol{k}_2\, \overline{\mathring{\boldsymbol{a}}(\boldsymbol{k}_2)\mathring{\boldsymbol{a}}^{\dagger}(\boldsymbol{k}_1)}\, \mathrm{e}^{\mathrm{i}(\boldsymbol{k}_1-\boldsymbol{k}_2)\cdot\boldsymbol{x}}\, \mathrm{e}^{-\mathrm{i}(\boldsymbol{k}_1+\boldsymbol{k}_2)\cdot\boldsymbol{s}/2}$$
$$= \int \mathrm{d}\bar{\boldsymbol{k}}\mathrm{d}\boldsymbol{k}'\, \overline{\mathring{\boldsymbol{a}}(\bar{\boldsymbol{k}}-\boldsymbol{k}'/2)\mathring{\boldsymbol{a}}^{\dagger}(\bar{\boldsymbol{k}}+\boldsymbol{k}'/2)}\, \mathrm{e}^{\mathrm{i}\boldsymbol{k}'\cdot\boldsymbol{x}}\, \mathrm{e}^{-\mathrm{i}\bar{\boldsymbol{k}}\cdot\boldsymbol{s}}. \tag{C7}$$

For this to be independent of $\boldsymbol{x}$ one needs

$$\overline{\mathring{\boldsymbol{a}}(\bar{\boldsymbol{k}}-\boldsymbol{k}'/2)\mathring{\boldsymbol{a}}^{\dagger}(\bar{\boldsymbol{k}}+\boldsymbol{k}'/2)} \propto \delta(\boldsymbol{k}'). \tag{C8}$$

Hence after statistical averaging and integrating out the delta, one gets the required relationship:

$$\bar{\mathbf{B}}_{\boldsymbol{vv}}(\boldsymbol{k}) = \omega_{\mathrm{pe}}^{-1}\omega_{\boldsymbol{k}}\bar{\mathbf{W}}_{\boldsymbol{vv}}(\boldsymbol{k}). \tag{C9}$$

REFERENCES

Abu-Shawareb, H., *et al.* 2022 Lawson criterion for ignition exceeded in an inertial fusion experiment. *Phys. Rev. Lett.* **129**, 075001.

Abu-Shawareb, H., *et al.* 2024 Achievement of target gain larger than unity in an inertial fusion experiment. *Phys. Rev. Lett.* **132** (6), 065102.

Bates, J.W., Follett, R.K., Shaw, J.G., Obenschain, S.P., Myatt, J.F., Weaver, J.L., Wolford, M.F., Kehne, D.M., Myers, M.C. & Kessler, T.J. 2023 Suppressing parametric instabilities in direct-drive inertial-confinement-fusion plasmas using broadband laser light. *Phys. Plasmas* **30** (5), 052703.

Bodner, S.E. 2023 Comparison of an argon-fluoride gas laser with a solid-state laser for application to laser fusion energy. *J. Fusion Energy* **42** (2), 33.

Brandão, B., Santos, J.E., Trines, R.M.G.M., Bingham, R. & Silva, L.O. 2021 Bandwidth effects in stimulated brillouin scattering driven by partially incoherent light. *Plasma Phys. Control. Fusion* **63** (9), 094003.

Campbell, E.M., *et al.* 2021 Direct-drive laser fusion: status, plans and future. *Phil. Trans. R. Soc.* A **379** (2189), 20200011.

Connaughton, C., Nazarenko, S. & Quinn, B. 2015 Rossby and drift wave turbulence and zonal flows: the Charney–Hasegawa–Mima model and its extensions. *Phys. Rep.* **604**, 1–71.

Craxton, R.S., *et al.* 2015 Direct-drive inertial confinement fusion: a review. *Phys. Plasmas* **22** (11), 110501.

Dodin, I.Y. 2022 Quasilinear theory for inhomogeneous plasma. *J. Plasma Phys.* **88** (4), 905880407.

https://doi.org/10.1017/S0022377824000953 Published online by Cambridge University Press

DORRER, C., HILL, E.M. & ZUEGEL, J.D. 2020 High-energy parametric amplification of spectrally incoherent broadband pulses. *Opt. Express* **28** (1), 451–471.

DORRER, C., SPILATRO, M., HERMAN, S., BORGER, T. & HILL, E.M. 2021 Broadband sum-frequency generation of spectrally incoherent pulses. *Opt. Express* **29** (11), 16135–16152.

DUBOIS, D.F. 2000 From Kadanoff-Baym equations to plasma turbulence. In *Progress in Nonequilibrium Green's Functions*, pp. 112–143. World Scientific.

DUBOIS, D.F. & BEZZERIDES, B. 1976 Nonlinear theory of parametric instabilities in plasmas. *Phys. Rev.* A **14** (5), 1869.

DUBOIS, D.F., BEZZERIDES, B. & ROSE, H.A. 1992 Collective parametric instabilities of many overlapping laser beams with finite bandwidth. *Phys. Fluids* B*: Plasma Phys*. **4** (1), 241–251.

DUBOIS, D.F., ROSE, H.A. & RUSSELL, D. 1996 Saturation of radiation-induced parametric instabilities by excitation of Langmuir turbulence. *Phys. Scr*. **1996** (T63), 16.

DUBOIS, D.F., RUSSELL, D.A. & ROSE, H.A. 1995 Saturation spectra of the two-plasmon decay instability. *Phys. Rev. Lett*. **74** (20), 3983.

FOLLETT, R.K., MYATT, J.F., SHAW, J.G., MICHEL, D.T., SOLODOV, A.A., EDGELL, D.H., YAAKOBI, B. & FROULA, D.H. 2017 Simulations and measurements of hot-electron generation driven by the multibeam two-plasmon-decay instability. *Phys. Plasmas* **24** (10), 102134.

FOLLETT, R.K., SHAW, J.G., MYATT, J.F., DORRER, C., FROULA, D.H. & PALASTRO, J.P. 2019 Thresholds of absolute instabilities driven by a broadband laser. *Phys. Plasmas* **26** (6), 062111.

FOLLETT, R.K., SHAW, J.G., MYATT, J.F., WEN, H., FROULA, D.H. & PALASTRO, J.P. 2021 Thresholds of absolute two-plasmon-decay and stimulated raman scattering instabilities driven by multiple broadband lasers. *Phys. Plasmas* **28** (3), 032103.

FOLLETT, R.K., WEN, H., FROULA, D.H., TURNBULL, D. & PALASTRO, J.P. 2022 Independent-hot-spot approach to multibeam laser-plasma instabilities. *Phys. Rev.* E **105** (6), L063201.

GARNIER, J. 1999 Statistics of the hot spots of smoothed beams produced by random phase plates revisited. *Phys. Plasmas* **6** (5), 1601–1610.

GOODMAN, J.W. 2015 *Statistical Optics*. John Wiley & Sons.

KROMMES, J.A. 2002 Fundamental statistical descriptions of plasma turbulence in magnetic fields. *Phys. Rep*. **360** (1-4), 1–352.

KROMMES, J.A. 2015 A tutorial introduction to the statistical theory of turbulent plasmas, a half-century after Kadomtsev's Plasma Turbulence and the resonance-broadening theory of Dupree and Weinstock. *J. Plasma Phys*. **81** (6), 205810601.

KROMMES, J.A. & PARKER, J.B. 2019 Statistical closures and zonal flows. In *Zonal Jets: Phenomenology, Genesis, and Physics* (ed. B. Galperin & P.L. Read), pp. 309–331. Cambridge University Press.

KRUER, W. 2019 *The Physics of Laser Plasma Interactions*. CRC Press.

LAVAL, G., PELLAT, R. & PESME, D. 1976 Absolute parametric excitation by an imperfect pump or by turbulence in an inhomogeneous plasma. *Phys. Rev. Lett*. **36** (4), 192.

LAVAL, G., PELLAT, R., PESME, D., RAMANI, A., ROSENBLUTH, M.N. & WILLIAMS, E.A. 1977 Parametric instabilities in the presence of space-time random fluctuations. *Phys. Fluids* **20** (12), 2049–2057.

LIU, C.S. & ROSENBLUTH, M.N. 1976 Parametric decay of electromagnetic waves into two plasmons and its consequences. *Phys. Fluids* **19** (7), 967–971.

LU, L. 1988 Framework of parametric instabilities in the presence of space-time fluctuations in homogeneous and inhomogenous plasmas. I. Theory. *Phys. Fluids* **31** (11), 3362–3370.

LU, L. 1989 Framework of the parametric instabilities in the presence of space-time fluctuations in homogeneous and inhomogeneous plasma. II. Applications. *Phys. Fluids* B*: Plasma Phys*. **1** (8), 1605–1615.

MACHACEK, A.C. & WARK, J.S. 2001 A versatile matrix-based solution for the two plasmon decay instability. *Phys. Plasmas* **8** (3), 704–712.

MCDONALD, S.W. 1988 Phase-space representations of wave equations with applications to the eikonal approximation for short-wavelength waves. *Phys. Rep*. **158** (6), 337–416.

MICHEL, D.T., MAXIMOV, A.V., SHORT, R.W., DELETTREZ, J.A., EDGELL, D., HU, S.X., IGUMENSHCHEV, I.V., MYATT, J.F., SOLODOV, A.A., STOECKL, C., YAAKOBI, B. & FROULA, D.H.2013 Measured hot-electron intensity thresholds quantified by a two-plasmon-decay resonant common-wave gain in various experimental configurations. *Phys. Plasmas* **20** (5), 055703.

https://doi.org/10.1017/S0022377824000953 Published online by Cambridge University Press

MICHEL, P. 2023 *Introduction to Laser-Plasma Interactions*, 1st edn. Springer.

MYATT, J.F., FOLLETT, R.K., SHAW, J.G., EDGELL, D.H., FROULA, D.H., IGUMENSHCHEV, I.V. & GONCHAROV, V.N. 2017 A wave-based model for cross-beam energy transfer in direct-drive inertial confinement fusion. *Phys. Plasmas* **24** (5), 056308.

MYATT, J.F., ZHANG, J., SHORT, R.W., MAXIMOV, A.V., SEKA, W., FROULA, D.H., EDGELL, D.H., MICHEL, D.T., IGUMENSHCHEV, I.V., HINKEL, D.E., MICHEL, P. & MOODY, J.D. 2014 Multiple-beam laser–plasma interactions in inertial confinement fusion. *Phys. Plasmas* **21** (5), 055501.

NAZARENKO, S. 2011 *Wave Turbulence*, 1st edn. Springer.

OBENSCHAIN, S.P., LUHMANN, N.C. & GREILING, P.T. 1976 Effects of finite-bandwidth driver pumps on the parametric-decay instability. *Phys. Rev. Lett*. **36** (22), 1309.

PADDOCK, R.W., MARTIN, H., RUSKOV, R.T., SCOTT, R.H.H., GARBETT, W., HAINES, B.M., ZYLSTRA, A.B., ABOUSHELBAYA, R., MAYR, M.W., SPIERS, B.T., WANG, R.H.W. & NORREYS, P.A. 2021 One-dimensional hydrodynamic simulations of low convergence ratio direct-drive inertial confinement fusion implosions. *Phil. Trans. R. Soc.* A *Math. Phys. Engng Sci*. **379** (2189), 20200224.

PADDOCK, R.W., MARTIN, H., RUSKOV, R.T., SCOTT, R.H.H., GARBETT, W., HAINES, B.M., ZYLSTRA, A.B., CAMPBELL, E.M., COLLINS, T.J.B., CRAXTON, R.S., THOMAS, C.A., GONCHAROV, V.N., ABOUSHELBAYA, R., FENG, Q.S., VON DER LEYEN, M.W., OUATU, I., SPIERS, B.T., TIMMIS, R., WANG, R.H.W. & NORREYS, P.A. 2022 Pathways towards break even for low convergence ratio direct-drive inertial confinement fusion. *J. Plasma Phys*. **88** (3), 905880314.

PARKER, J.B. 2014 Zonal flows and turbulence in fluids and plasmas. PhD thesis, Princeton University.

PARKER, J.B. 2016 Dynamics of zonal flows: failure of wave-kinetic theory, and new geometrical optics approximations. *J. Plasma Phys*. **82** (6), 595820602.

PESME, D., BERGER, R.L., WILLIAMS, E.A., BOURDIER, A. & BORTUZZO-LESNE, A. 1992 A statistical description of parametric instabilities with an incoherent pump; effet de l'incohérence spatiale induite sur les instabilités paramétriques. *Tech. Rep.* CEA-N-2692. Commissariat à l'énergie atomique et aux énergies alternatives. arXiv:0710.2195.

ROSE, H.A. & DUBOIS, D.F. 1993 Statistical properties of laser hot spots produced by a random phase plate. *Phys. Fluids* B*: Plasma Phys*. **5** (2), 590–596.

ROSENBERG, M.J., SOLODOV, A.A., MYATT, J.F., SEKA, W., MICHEL, P., HOHENBERGER, M., SHORT, R.W., EPSTEIN, R., REGAN, S.P., CAMPBELL, E.M., CHAPMAN, T., GOYON, C., RALPH, J.E., BARRIOS, M.A., MOODY, J.D. & BATES, J.W. 2018 Origins and scaling of hot-electron preheat in ignition-scale direct-drive inertial confinement fusion experiments. *Phys. Rev. Lett*. **120**, 055001.

RUIZ, D.E., GLINSKY, M.E. & DODIN, I.Y. 2019 Wave kinetic equation for inhomogeneous drift-wave turbulence beyond the quasilinear approximation. *J. Plasma Phys*. **85** (1), 905850101.

RUIZ, D.E., PARKER, J.B., SHI, E.L. & DODIN, I.Y. 2016 Zonal-flow dynamics from a phase-space perspective. *Phys. Plasmas* **23** (12), 122304.

SANTOS, J.E., SILVA, L.O. & BINGHAM, R. 2007 White-light parametric instabilities in plasmas. *Phys. Rev. Lett*. **98** (23), 235001.

SANTOS, J.P. & SILVA, L.O. 2005 Wigner-moyal description of free variable mass Klein-Gordon fields. *J. Math. Phys*. **46** (10), 102901.

SCHMITT, A.J. & OBENSCHAIN, S.P. 2023*a* The importance of laser wavelength for driving inertial confinement fusion targets. I. Basic physics. *Phys. Plasmas* **30** (1), 012701.

SCHMITT, A.J. & OBENSCHAIN, S.P. 2023*b* The importance of laser wavelength for driving inertial confinement fusion targets. II. Target design. *Phys. Plasmas* **30** (1), 012702.

SEKA, W., MYATT, J.F., SHORT, R.W., FROULA, D.H., KATZ, J., GONCHAROV, V.N. & IGUMENSHCHEV, I.V. 2014 Nonuniformly driven two-plasmon-decay instability in direct-drive implosions. *Phys. Rev. Lett*. **112** (14), 145001.

SILVA, L.O. & BINGHAM, R. 2013 *Laser-Plasma Interactions and Applications*. Theory of Underdense Laser-Plasma Interactions with Photon Kinetic Theory, pp. 3–18. Springer.

SIMON, A., SHORT, R.W., WILLIAMS, E.A. & DEWANDRE, T. 1983 On the inhomogeneous two-plasmon instability. *Phys. Fluids* **26** (10), 3107–3118.

SMOLYAKOV, A.I., DIAMOND, P.H. & SHEVCHENKO, V.I. 2000 Zonal flow generation by parametric instability in magnetized plasmas and geostrophic fluids. *Phys. Plasmas* **7** (5), 1349–1351.

THOMSON, J.J. 1975 Finite-bandwidth effects on the parametric instability in an inhomogeneous plasma. *Nucl. Fusion* **15** (2), 237.

THOMSON, J.J. & KARUSH, J.I. 1974 Effects of finite-bandwidth driver on the parametric instability. *Phys. Fluids* **17** (8), 1608–1613.

TRACY, E.R., BRIZARD, A.J., RICHARDSON, A.S. & KAUFMAN, A.N. 2014 *Ray Tracing and Beyond: Phase Space Methods in Plasma Wave Theory*. Cambridge University Press.

TRICKEY, W., GONCHAROV, V.N., BETTI, R., CAMPBELL, E.M., COLLINS, T.J.B. & FOLLETT, R.K. 2024 The physics of gain relevant to inertial fusion energy target designs. *Phys. Plasmas* **31** (1), 012702.

TRINES, R., BINGHAM, R., DUNLOP, M.W., VAIVADS, A., DAVIES, J.A., MENDONÇA, J.T., SILVA, L.O. & SHUKLA, P.K. 2007 Spontaneous generation of self-organized solitary wave structures at Earth's magnetopause. *Phys. Rev. Lett*. **99** (20), 205006.

TRINES, R., BINGHAM, R., SILVA, L.O., MENDONÇA, J.T., SHUKLA, P.K. & MORI, W.B. 2005 Quasiparticle approach to the modulational instability of drift waves coupling to zonal flows. *Phys. Rev. Lett*. **94** (16), 165002.

TRINES, R.M.G.M., BINGHAM, R., SILVA, L.O., MENDONÇA, J.T., SHUKLA, P.K., MURPHY, C.D., DUNLOP, M.W., DAVIES, J.A., BAMFORD, R., VAIVADS, A. & NORREYS, P.A. 2009 Applications of the wave kinetic approach: from laser wakefields to drift wave turbulence. *Phys. Plasmas* **16** (5), 055904.

TSIOLIS, V., ZHOU, Y. & DODIN, I.Y. 2020 Structure formation in turbulence as an instability of effective quantum plasma. *Phys. Lett.* A **384** (18), 126377.

TURNBULL, D., BONI, R., COLAITIS, A., DORRER, C., EDGELL, D., FOLLETT, R., FROULA, D., GONCHAROV, V., HABERBERGER, D., HILL, E., KATZ, J., MILDER, A.L., PALASTRO, J.P., SHAH, R., SHVYDKY, A., SOLODOV, A., & ZUEGEL, J. 2023 Thomas H. Stix award for outstanding early career contributions to plasma physics research: developing broadband laser drivers for a step change in ICF performance through laser-plasma instability mitigation. *Bulletin of the American Physical Society*, APS Division of Plasma Physics Meeting 2023, DI02.0001.

TURNBULL, D., MAXIMOV, A.V., EDGELL, D.H., SEKA, W., FOLLETT, R.K., PALASTRO, J.P., CAO, D., GONCHAROV, V.N., STOECKL, C. & FROULA, D.H. 2020 Anomalous absorption by the two-plasmon decay instability. *Phys. Rev. Lett*. **124** (18), 185001.

VU, H.X., DUBOIS, D.F., MYATT, J.F. & RUSSELL, D.A. 2012*a* Hot-electron production and suprathermal heat flux scaling with laser intensity from the two-plasmon–decay instability. *Phys. Plasmas* **19** (10), 102703.

VU, H.X., DUBOIS, D.F., RUSSELL, D.A. & MYATT, J.F. 2012*b* Hot-electron generation by 'cavitating' Langmuir turbulence in the nonlinear stage of the two-plasmon–decay instability. *Phys. Plasmas* **19** (10), 102708.

YAN, R., MAXIMOV, A.V. & REN, C. 2010 The linear regime of the two-plasmon decay instability in inhomogeneous plasmas. *Phys. Plasmas* **17** (5), 052701.

ZHANG, J., MYATT, J.F., SHORT, R.W., MAXIMOV, A.V., VU, H.X., DUBOIS, D.F. & RUSSELL, D.A. 2014 Multiple beam two-plasmon decay: linear threshold to nonlinear saturation in three dimensions. *Phys. Rev. Lett*. **113** (10), 105001.

ZHU, H. 2020 Phase-space theory of drift wave–zonal flow interactions and the dimits shift. PhD thesis, Princeton University.

ZHU, H. & DODIN, I.Y. 2021 Wave-kinetic approach to zonal-flow dynamics: recent advances. *Phys. Plasmas* **28** (3), 032303.

ZHU, H., ZHOU, Y. & DODIN, I.Y. 2020 Theory of the tertiary instability and the dimits shift from reduced drift-wave models. *Phys. Rev. Lett*. **124**, 055002.

ZYLSTRA, A.B. 2022 Burning plasma achieved in inertial fusion. *Nature* **601** (7894), 542–548.

https://doi.org/10.1017/S0022377824000953 Published online by Cambridge University Press